CHEMICAL REVIEWS

Review

pubs.acs.org/CR

Liquid Metal Batteries: Past, Present, and Future

Hojong Kim, Dane A. Boysen, Jocelyn M. Newhouse, Brian L. Spatocco, Brice Chung, Paul J. Burke, David J. Bradwell, Kai Jiang, Alina A. Tomaszowska, Kangli Wang, Weifeng Wei, Luis A. Ortiz, Salvador A. Barriga, Sophie M. Poizeau, and Donald R. Sadoway*

Department of Materials Science and Engineering, Massachusetts Institute of Technology, 77 Massachusetts Avenue, Cambridge, Massachusetts 02139-4307, United States

CONTENTS

1. INTRODUCTION

The evolution of the liquid metal battery is a story of a novel technology originally conceived in a different economic and political climate to provide flexibility in addressing the constraints of a society just entering the nuclear age and with aspirations to electrify the everyday experience. Ironically, it is these same massive research projects that receded into obscurity that can now be resurrected and reinvented as an exciting opportunity for addressing society's ambitions for both sustainable and environmentally benign energy. In contrast to the public's demand for the constant improvement of high-performance lithium-ion batteries for portable electronics,[1] liquid metal batteries are instead the story of a society catching up with a technology far ahead of its time.

The story of the all-liquid electrochemical cell begins nearly a century ago with advances in the electrolytic production of ultrahigh-purity aluminum. Building upon those early advances in classical electrometallurgy, four decades later the U.S. government began to fund pioneering work at a few of the nation's top industrial and national laboratories to develop all-liquid cells for energy storage applications. Motivated by the Cold War battle for technological supremacy, intensive research on these thermally and electrically rechargeable all-liquid energy storage cells continued in the U.S. throughout the next decade, only to be abandoned as efforts shifted toward higher-energy-density rechargeable cells with immobilized components better suited for automotive applications. After a nearly 40-year hiatus, the rapid deployment of renewable energy technologies, such as wind and solar power, has hastened the demand for low-cost, long-life, large-scale energy

Received: May 22, 2012
Published: November 27, 2012

   dx.doi.org/10.1021/cr300205k | Chem. Rev. 2013, 113, 2075–2099

storage and renewed interest in the rechargeable three-liquid-layer galvanic cell—the liquid metal battery.

1.1. Description

A liquid metal battery comprises two liquid metal electrodes separated by a molten salt electrolyte that self-segregate into three layers based upon density and immiscibility (Figure 1).

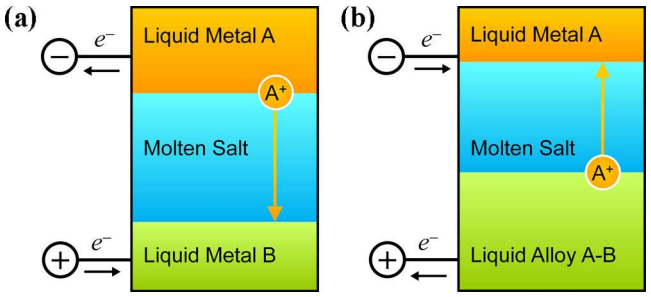

Figure 1. Schematic diagram of a liquid metal battery upon (a) discharging and (b) charging.

1												13	14	15	16	17	18
H	2																He
Li	Be											B	C	N	O	F	Ne
Na	Mg	3	4	5	6	7	8	9	10	11	12	Al	Si	P	S	Cl	Ar
K	Ca	Sc	Ti	V	Cr	Mn	Fe	Co	Ni	Cu	Zn	Ga	Ge	As	Se	Br	Kr
Rb	Sr	Y	Zr	Nb	Mo	Tc	Ru	Rh	Pd	Ag	Cd	In	Sn	Sb	Te	I	Xe
Cs	Ba		Hf	Ta	W	Re	Os	Ir	Pt	Au	Hg	Tl	Pb	Bi	Po	At	Rn

Figure 2. Negative (orange) and positive (green) electrode material candidates for liquid metal batteries.

The compositions of the liquid metal electrodes, highlighted in the periodic table presented in Figure 2, are constrained according to the following three requirements:

(1) liquid at practical temperatures, that is, the melting temperature should be less than 1000 °C and the boiling point greater than 25 °C (T_b > 25 °C, T_m < 1000 °C)

(2) electrically conductive, with a minimum electronic conductivity greater than the ionic conductivity of a typical molten salt electrolyte (σ > 1 S cm^{-1})

(3) nonradioactive, that is, available in the form of a naturally occurring, stable isotope

Candidate electrode materials are preliminarily sorted into either positive or negative electrodes by the deposition potential of the candidate electrode material from aqueous solution[2] (Figure 3); however, since liquid metal batteries use molten salt electrolytes, these deposition potentials are not strictly comparable. Electrode materials with a deposition potential more negative than −2.0 V are negative electrodes (A metals) and those with potential more positive than −1.0 V are positive electrodes (B metals), with aluminum being unique in that it could be either. Alternately, one can sort elements based upon their electronegativity: the more electropositive metals being candidates for the negative electrode and the more electronegative metals (including the semimetals) being candidates for the positive electrode. The idea is to pair a strong electron donor with a strong electron acceptor while avoiding nonmetals in the choice of the latter.

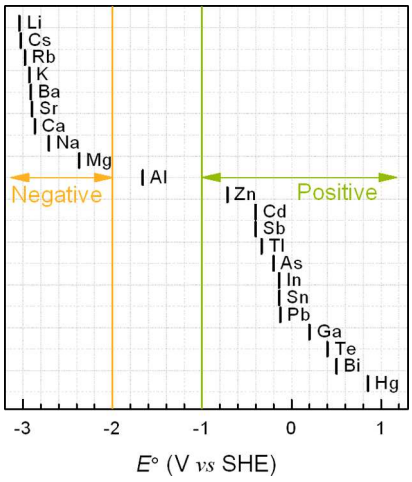

Figure 3. Deposition potentials versus the standard hydrogen electrode (SHE) in aqueous electrolytes of candidate electrode species, from which candidate negative (orange) and positive (green) liquid metal battery electrode materials are selected.[2]

The strong interaction between metals A and B provides the thermodynamic driving force (cell voltage) for the liquid metal battery cell. Upon discharge the negative electrode layer reduces in thickness, as metal A is electrochemically oxidized ($A \rightarrow A^{z+} + ze^-$), and the cations are conducted across the molten salt electrolyte to the positive electrode as electrons are released to an external circuit, Figure 1a. Simultaneously, the positive electrode layer grows in thickness, as the cations are electrochemically reduced to form a liquid A−B alloy [$A^{z+} + ze^- \rightarrow$ A(in B)]. This process is reversed upon charging, Figure 1b.

1.2. Advantages and Disadvantages

Liquidity endows liquid metal batteries with superior kinetics and transport properties. The operating voltage of any electrochemical cell, E_{cell}, deviates from the equilibrium cell potential, $E_{cell,eq}$, based upon current density, j, dependent losses or voltage inefficiencies, $\eta(j)$, such that $E_{cell}(j) = E_{cell,eq} - \sum_i \eta_i(j)$. Typical voltage inefficiencies include (1) charge transfer losses, η_{ct}, resulting from sluggish electrode kinetics, (2) ohmic losses, η_{ohm}, arising from the electrical resistivity of the cell electrolyte, electrodes, and current collectors, and (3) mass transport, η_{mt}, losses caused by slow diffusion of reactants to and products away from the electrode−electrolyte interface.[3,4] Liquid metal batteries boast ultrafast electrode charge-transfer kinetics due to liquid−liquid electrode−electrolyte interfaces, high rate capability, and low ohmic losses enabled by highly conductive molten salt electrolytes (up to 3 S cm^{-1}), and rapid mass transport of reactants and products to and from the electrode−electrolyte interface by liquid-state diffusion. In combination, these properties allow liquid metal batteries to operate with relatively high voltage efficiencies at high current densities.

Liquid metal batteries also have the potential of being low-cost because many of the candidate electrode materials are earth-abundant and inexpensive. Moreover, the natural self-segregation of the active liquid components allows simpler, lower-cost cell fabrication compared with that of conventional batteries. Finally, perhaps the most attractive feature of these batteries is the continuous creation and annihilation of the

dx.doi.org/10.1021/cr300205k | Chem. Rev. 2013, 113, 2075−2099

liquid metal electrodes upon charge−discharge cycling. This feature grants liquid metal batteries the potential for unprecedented cycle life by rendering them immune to microstructural electrode degradation mechanisms that limit the cycle life of a conventional battery.[5,6] When taken together, low cost of materials, simple assembly, and the potential for long lifetimes position liquid metal batteries particularly well for competition in the grid-storage market.

Despite these advantages, liquid metal batteries possess some disadvantages, which make them unsuitable for use in portable applications. These include elevated operating temperatures (generally >200 °C), low theoretical specific energy density (typically <200 Wh kg^{-1}), comparatively low equilibrium cell voltages (typically <1.0 V), highly corrosive active cell components, and high self-discharge rates for some chemistries due to metallic solubility of the electrode species in the molten salt electrolyte. Moreover, three liquid layers make battery operation sensitive to motion and potentially hazardous should the liquid electrodes touch, leading to a short-circuited cell and rapid heat generation.

1.3. Applications

High-temperature operation and all-liquid components restrict liquid metal batteries to stationary applications; however, the promise of low-cost, scalable, and high rate capable energy storage makes liquid metal batteries prime candidates for grid-scale energy storage (0.1−1.0 GWh). Today, grid-scale energy storage capacity represents less than 6% (130 GW) of global electricity generation, and demand is likely to increase as the need for off-grid storage grows due to market penetration of intermittent renewable power sources, increased electrification, advancements in smart grid technology, and deployment of electric vehicles.[7] However, in the absence of grid-scale electrical energy storage, power providers must continuously adjust output levels to meet fluctuating demand, causing a wide-range of operational and infrastructural inefficiencies.

Grid-scale energy storage requirements can be broadly classified into either energy or power applications. Energy applications, such as storing excess wind energy during periods of low power demand and providing power during periods of high demand, require long discharge times, typically several hours. By contrast, power applications, such as capturing the energy produced by a gust of wind, frequency regulation, and spinning reserves, require the ability to store large inputs of energy for short periods of time (seconds to minutes). As can be seen from Figure 4a, most technologies are more economical for either energy ($ kWh^{-1}) or power ($ kW^{-1}) applications;[8−10] however, the high rate capability of liquid metal batteries could allow them to serve both purposes, enabling dual-use applications and more attractive economics.

For grid-scale energy storage, liquid metal batteries must be cost-competitive with incumbent technologies.[7] Detailed cost−benefit analyses of existing technologies can be found elsewhere;[7−9,11] however, a first-order approximation is made here in an attempt to capture the essential metrics and enable the comparison of this nascent technology to more established energy storage technologies. In Figure 4b, the levelized cost or capital cost normalized by the cycle life and energy efficiency (cost × $cycles^{-1}$ × $efficiency^{-1}$) of grid-scale energy storage technologies is plotted against the globally installed capacity.[9] The trend is clear: low-cost technologies are preferred, even if they have very low energy and power densities and are geographically constrained (e.g., pumped hydroelectric and compressed air energy storage). Competing with existing energy storage technologies such as these is a major challenge for electrochemical systems, even though batteries offer the benefit of geographic flexibility and unfettered deployability. To a first approximation, a levelized cost of 5¢ kWh^{-1} cyc^{-1} would allow liquid metal batteries to be competitive with incumbent energy storage technologies. For example, a battery with a cost of $400 kWh^{-1}, lifetime of 10 000 cycles, and energy efficiency of 80% would meet the 5¢ kWh^{-1} cyc^{-1} price point. This levelized cost estimate is useful in identifying economically viable chemistries for liquid metal batteries and gauging their potential as a competitive grid-scale energy storage technology. For a target levelized energy cost of 5¢ kWh^{-1} cyc^{-1}, in this review, we assume a battery life of 10 000 cycles, an energy efficiency of 80%, and a materials cost of one-fourth of a total battery system to arrive at a target battery materials cost of under $100 kWh^{-1}. This metric will serve as a guide later in selecting promising low-cost electrode materials.

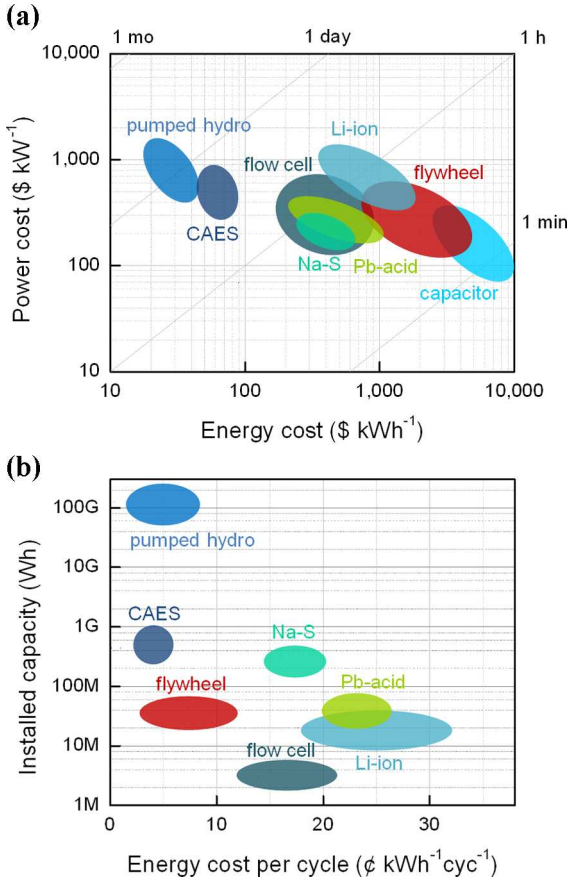

Figure 4. (a) Cost of power versus energy for various energy storage technologies, where CAES stands for compressed air energy storage (data from refs 8−10) and (b) globally installed energy storage capacity versus cycle normalized cost of energy (data from ref 9).

2. PAST WORK

The history of all-liquid electrochemical cells dates back to the turn of the last century with roots in the development of classical electrometallurgy and begins with advances resulting in the development of the three-liquid-layer Hoopes cell at the Aluminum Company of America (Alcoa) in the 1920s for the electrolytic production of high-purity aluminum.[12] Forty years later, the three-liquid-layer cell re-emerged as one variant of the

dx.doi.org/10.1021/cr300205k | Chem. Rev. 2013, 113, 2075−2099

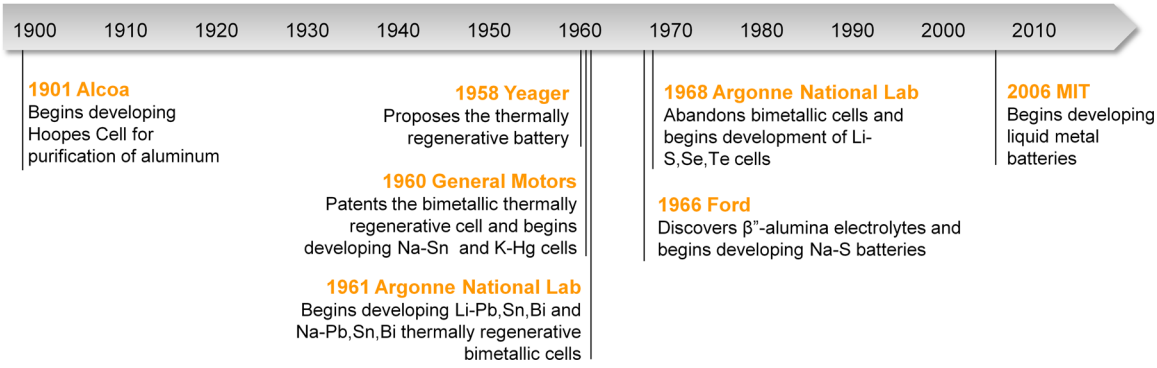

Figure 5. Historical timeline of the development of the three-liquid-layer electrochemical cell and liquid metal battery.

thermally regenerative battery, known as the bimetallic cell. Bimetallic cells enjoyed over a decade of intense research before they were eventually abandoned for higher energy density batteries for mobile applications. A high-level timeline of the development of the liquid metal batteries is shown in Figure 5.

2.1. Hoopes Cells

The first all-liquid electrochemical cell originated in the development of electrolytic methods for the production of high-purity metals. In 1922, Hoopes and co-workers at Alcoa filed several patents on the production of high-purity aluminum using a three-liquid-layer cell comprised of a high-density Cu–Al alloy (30–70 mol %, plus various impurities such as Fe, Si, etc.) bottom electrode and a low-density, high-purity liquid aluminum (>99.97 mass %) top electrode; separated by a molten salt electrolyte, as shown in Figure 6.[12−14] Immediately

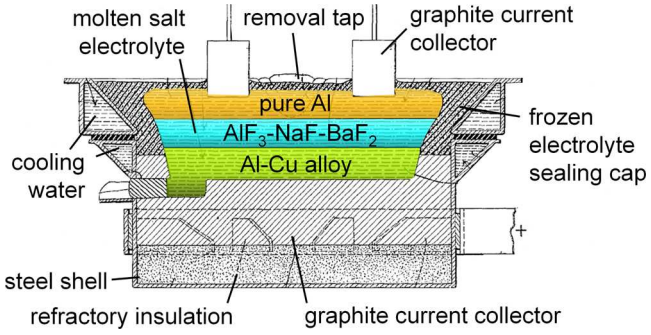

Figure 6. Diagram of a Hoopes cell from a 1925 Alcoa patent that describes a three-liquid-layer electrolytic cell for the purification of aluminum.[12] Adapted from Alcoa patent, US Patent No. 1,534,315.

apparent is the physical similarity of the Hoopes cell to a liquid metal battery (Figure 1), except that in a Hoopes cell high-purity aluminum is produced only upon "charging" and then siphoned off. In theory, the cell could be operated as a rechargeable battery, albeit a poor one with an equilibrium cell voltage of under 30 mV.[15] Hoopes cells are still in operation today and have logged more than 20 years of continuous operation without retrofitting.[16]

2.2. Thermally Regenerative Batteries

It was not until the 1960s that the three-liquid-layer electrochemical cell became of interest for energy storage and conversion applications. In 1958, Yeager proposed the concept of a "thermally regenerative closed cycle battery" that could convert heat into chemically stored energy, which in turn could be converted into electricity, Figure 7a.[17] This device would electrochemically discharge like a normal battery cell to

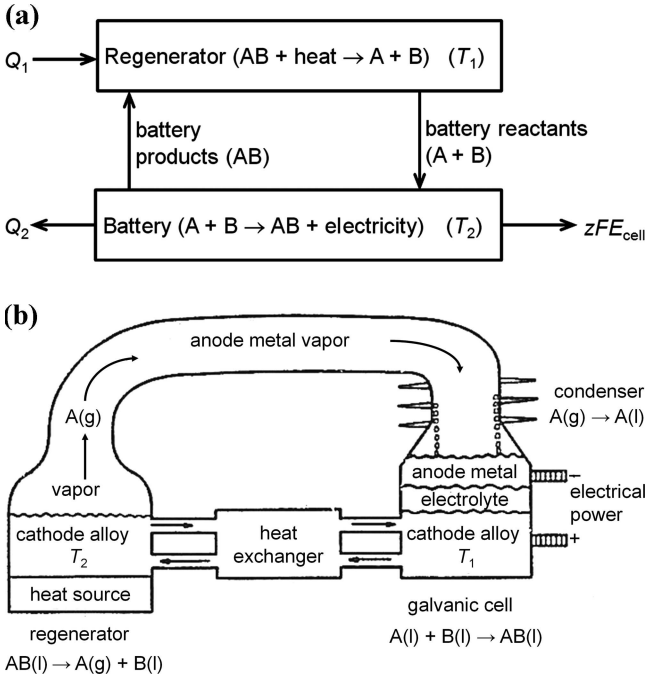

Figure 7. (a) Schematic drawing of Yeager's original 1958 concept of a thermally regenerative battery.[17] (b) Schematic diagram from Argonne National Laboratory of a thermally regenerative bimetallic cell. Reprinted with permission from ref 37. Copyright 1967 Argonne National Laboratory.

produce compound AB and electricity (A + B → AB + electricity), but use thermal energy to recharge by thermochemically dissociating compound AB back into cell reactants A and B (AB + heat → A + B). Unlike a purely electrochemical cell, the thermally regenerative cell is subject to Carnot cycle efficiency limitations, such that the maximum efficiency is $\eta_{Carnot} = (T_1 - T_2)/T_1$, where T_1 and T_2 are the thermochemical regenerator and electrochemical cell operating temperatures, respectively.

In a decade of massive investments in nuclear energy and growing interest in solar energy (thermal energy sources), the capability of thermally regenerative cells to convert low-grade thermal energy into high-grade electrical energy on demand at reasonable theoretical efficiencies (η > 15%) and with no

dx.doi.org/10.1021/cr300205k | Chem. Rev. 2013, 113, 2075–2099

moving parts quickly gained widespread appeal and spawned research and development programs across the United States.

Over the next decade, two general types of thermally regenerative batteries emerged: (1) metal hydride or metal halide cells and (2) bimetallic cells. For metal hydride or halide cells, hydrogen or halogen gases (X_2 = H_2, F_2, Cl_2, Br_2, I_2) are electrochemically reacted with a liquid metal A to form a metal hydride or halide discharge product (AX) that is solvated in a molten salt electrolyte and subsequently thermochemically regenerated (dissociated) back into a hydrogen or halide gas and liquid metal. By contrast, in bimetallic cells an electropositive liquid metal A is reacted with an electronegative liquid metal B to form a molten metal alloy AB that is then thermally regenerated (distilled) through the preferential evaporation of reactant gas A from AB liquid product, as depicted in Figure 7b.

Of this body of work, only bimetallic cells exhibit the three-liquid-layer self-segregating structure relevant to this review. For a more comprehensive review of thermally regenerative cells that includes both cell types see Crouthamel and Recht (1967).[18] In the United States, large-scale research and development efforts were undertaken in the 1960s to develop bimetallic thermally regenerative cells at the General Motors Corporation, Argonne National Laboratory, and Atomics International (a division of North American Aviation).

2.3. Bimetallic Cells

2.3.1. General Motors Corporation. In 1960, Agruss at General Motors filed the first patent on thermally regenerative bimetallic cells, in which he describes essentially a liquid metal battery that is thermally "recharged".[19] General Motors began their research on Na−Sn liquid metal cells with a NaCl−NaI molten salt electrolyte, which they demonstrated electrochemical charge−discharge for over a month at 700 °C, achieving current densities up to 0.7 A cm^{-2} and Coulombic efficiencies of 95% at modest cell voltages of 0.33−0.43 V.[20−22] Later, they redirected the program toward the development of K−Hg thermally regenerative cells with KOH−KBr−KI molten salt electrolytes "because the kinetics of separating K−Hg were felt to be far superior to the earlier Na−Sn system."[22] Using a cell as depicted in Figure 8a, General Motors reversibly charged−discharged a K−Hg cell at a current density of 87 mA cm^{-2} and achieved Coulombic efficiencies of 90−95%. A sample charge−discharge plot is reproduced in Figure 8b. Using a three-cell K−Hg battery in conjunction with a thermal regenerative system, Agruss and Karas reported 60 h of successful operation at a power density of 48 mW cm^{-2} and thermal to electric energy conversion efficiency of ∼3%.[22,23] Results of General Motors' thermally and electrically rechargeable bimetallic cells are summarized in Tables 1 and 2, respectively.

2.3.2. Atomics International. Within the same decade, Atomics International undertook the development of Na−Hg bimetallic cells for application in a space power plant to convert heat from a compact nuclear reactor into electricity. The initial static cell tests (no flowing electrodes) at 510 °C were carried out using cells very similar to those used by General Motors (Figure 8a), only the ternary sodium halide molten salt electrolyte was immobilized within a solid ceramic matrix. The cell was then operated in conjunction with a thermal regenerator at 670−690 °C for nearly 1200 h; however, mercury corrosion ultimately led to system failure, these results are summarized in Table 1.[24−26] Despite these profound research efforts, both the work at Atomics International and

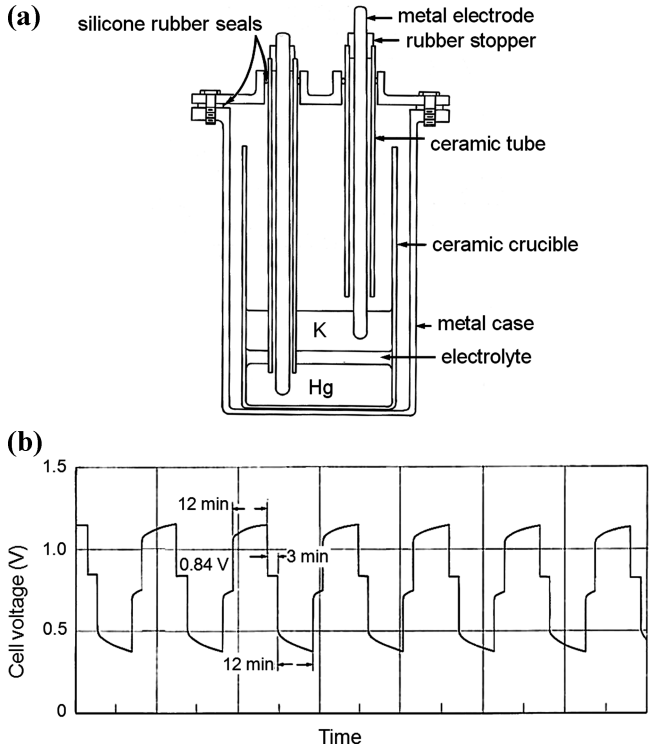

Figure 8. A K|KOH−KBr−KI|Hg differential density liquid metal cell developed at the General Motors Corporation: (a) schematic diagram and (b) plot of cell voltage versus time upon charge and discharge at 87 mA cm^{-2} and 300 °C with an 11.5 cm^2 electrode area and 1.5 cm electrolyte thickness. Reprinted with permission from ref 22. Copyright 1967 American Chemical Society.

General Motors fell into anonymity, going for decades without citation in the annals of contemporary scientific literature.

3.3.3. Argonne National Laboratory. From 1961 to 1967, Argonne National Laboratory carried out perhaps the most comprehensive work on bimetallic cells. The initial program focused primarily on the development of bimetallic cells for thermally regenerative batteries; however, the high electrical charge and discharge rate capability of these cells led researchers to believe that bimetallic cells were also attractive candidates for secondary cell applications.[27−38] Early work was devoted to Na and Li negative electrodes with Pb, Sb, and Bi positive electrodes, but later work moved toward the development of chalcogenide (S, Se, Te) positive electrodes. The research program at Argonne was extensive, spanning fundamental thermodynamic investigations of electrode couples, to the measurement of molten salt electrolyte properties, to the study of cell component corrosion, and to the design and testing of practical cells. Given the breadth of work carried out at Argonne, only some of the highlights are reviewed here; further details can be found in the literature.[31−60]

For sodium-based bimetallic cells, Argonne selected the lowest known melting point (530 °C) all-sodium ion ternary eutectic molten salt electrolyte (15:32:53 mol % NaF−NaCl−NaI), which has an ionic conductivity of ∼2.2 S cm^{-1} at 550 °C. Lead was selected over Bi and Sn for thermally regenerative cells because of simpler thermal distillation of the discharge product. A 28 Ah Na−Pb (30 mol % Na) thermally regenerative cell was successfully constructed and operated for a total of 45 h, while discharging continuously for several

dx.doi.org/10.1021/cr300205k | Chem. Rev. 2013, 113, 2075−2099

Table 1. Performance Results of Thermally Regenerative Bimetallic Cells

	unit	Na−Sn[22]	K−Hg[22]	Na−Hg[24−26]	Na−Pb[37]
electrolyte chemistry		NaCl−NaI	KOH−KBr−KI	Na halides−ceramic filler	NaF−NaCl−NaI
operating temperature	°C	625−650	325	490	575
regeneration temperature	°C	1000		670−690	875
electrode area	cm^2		1[a]	1[a]	45
interelectrode distance	cm				1.9
charge−discharge current	A	0.1		0.05−0.10	5
theoretical capacity	Ah				28
discharge capacity	Ah	0.025			∼16
power output	W		0.05−0.10	35	
open-circuit voltage	V	0.33−0.43	0.70−0.84	0.30−0.80	0.3−0.5
average discharge voltage	V	0.3			0.17
estimated efficiency	%	16	3[b]	7	<15
test duration	h	0.3	430	1200	45
organization[c]		GM	GM	AI	ANL

[a]Electrode area was unknown therefore assumed to be unity. [b]Measured efficiency. [c]Results obtained at General Motors (GM), Atomic International (AI), and Argonne National Laboratory (ANL).

Table 2. Performance results of secondary bimetallic cells

	unit	Na−Sn[22]	K−Hg[22,23]	Na−Bi[37]	Li−Te[37,42]
electrolyte chemistry		NaCl−NaI	KOH−KBr−KI	NaF−NaCl−NaI	LiF−LiCl−LiI
operating temperature	°C	700	325	580	480
electrode area	cm^2	1[a]	11.5	45	10
interelectrode distance	cm		1.5	0.4	0.5
charge−discharge current	A	0.7	1.0	30	20
theoretical capacity	Ah			15	1.55
discharge capacity	Ah		0.2	8.5	1.25
coulombic efficiency	%	95	90−95	80	90
open-circuit voltage	V	0.33−0.43	0.70−0.84	0.55−0.75	1.7−1.8
discharge voltage	V		0.4	0.3	1.3
test duration	h	744		12240	>300
organization[b]		GM	GM	ANL	ANL

[a]Unknown electrode area normalized to one. [b]Results obtained at General Motors (GM) and Argonne National Laboratory (ANL).

hours at 110 mA cm^{-2} and 170 mV at cell and regenerator temperatures of 575 °C and 875 °C (930 Pa), respectively.[37]

For secondary cells, Na−Bi was preferred because of a higher theoretical cell voltage. Several Na−Bi 15 Ah secondary cells were constructed using a design that featured an externally cooled silicone rubber seal and frozen electrolyte side-wall, as illustrated in Figure 9a. One of these cells was continuously operated for more than 17 months with no appreciable degradation in performance. Cells achieved charge−discharge current densities as high as 1.1 A cm^{-2} at 535−650 °C with a 0.4 cm thick electrolyte; however, high current densities prevented the cell from achieving its theoretical cell capacity upon discharge as a result of electrode diffusion limitations concomitant with the formation of intermetallic species at the electrode−electrolyte interface, Figure 9b. A relatively large self-discharge rate was observed in all sodium-based cells due to sodium solubility in the molten salt electrolyte, requiring charge rates greater than 110 mA cm^{-2} and limiting Coulombic efficiencies to less than 80% at 665 mA cm^{-2} and 565 °C.[37] Ultimately, the issue of sodium solubility in molten salt electrolytes that results in high self-discharge rates drove a shift toward the solid-state electrolyte sodium β''-alumina after its discovery at Ford Motor Company in 1966.[61−64]

For lithium-based bimetallic cells, Argonne investigated several binary and ternary lithium halide molten salt electrolytes, but the LiF−LiCl−LiI eutectic composition (12:29:59 mol %) which melts at 341 °C was preferred. In general, it was found that lithium halides melt about 200 °C lower than their sodium halide homologues. This is important because it allows lithium-based cells to operate at lower temperatures, provides for lower solubility of the electrode materials in the electrolyte, and significantly reduces cell self-discharge. Initial lithium-based cells were tested with Zn, Cd, Pb, Bi, Sn, and Te positive electrodes, and all were capable of operating at current densities in excess of 0.3 A cm^{-2}. Based upon thermodynamic investigations of the Li−Sn system, Argonne predicted that excellent separation of lithium from tin could be achieved with a galvanic cell at 327 °C and regenerator at 1023 °C with a system efficiency of nearly 30%. These predictions remain unverified because Li−Sn thermally regenerative systems were never constructed.[37]

Of the initial candidate couples tested, Li−Te exhibited the highest cell voltages (1.7−1.8 V) and was therefore deemed the most promising secondary cell electrode couple. Lithium−tellurium secondary cells were constructed in accordance with a design similar to that used for the Na−Bi cells (Figure 9a), operated at ∼480 °C, charged−discharged at massive current densities of up to 7 A cm^{-2} (Figure 10a), and displayed no signs of degradation after 300 h of operation. In contrast to the Na−Bi cells, the Li−Te cells exhibited consistent voltage discharge profiles even at current densities as high as 3 A cm^{-2}, Figure 10b.[37,42]

dx.doi.org/10.1021/cr300205k | Chem. Rev. 2013, 113, 2075−2099

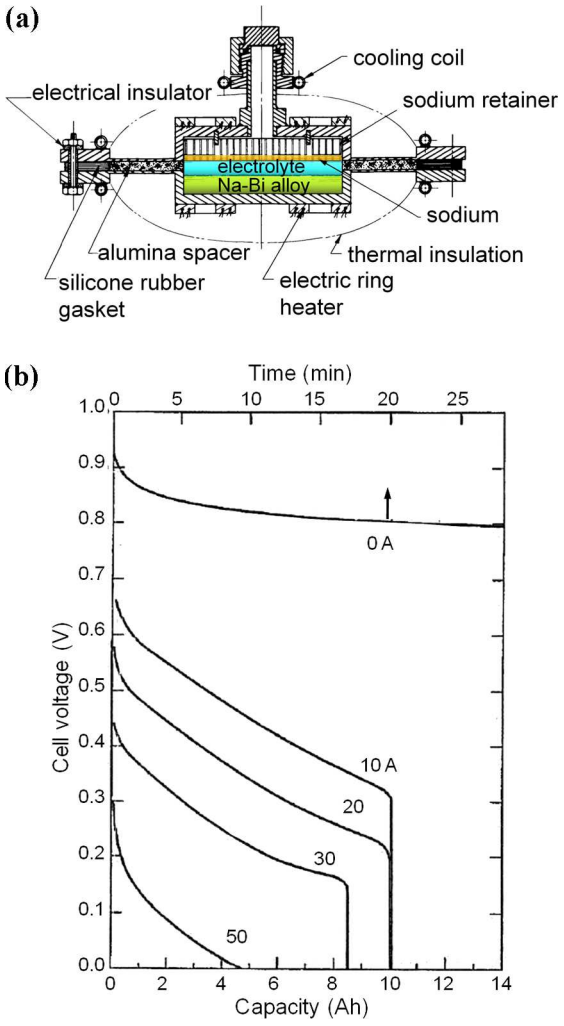

Figure 9. A NaINaF–NaCl–NaI|Bi bimetallic secondary cell developed at Argonne National Laboratory: (a) schematic of a 20 Ah nominal capacity cell with externally cooled seal and (b) plot of cell voltage versus capacity at various constant-current discharge rates of a cell at 580 °C with a 45 cm^2 electrode area and 0.4 cm interelectrode distance. Reprinted with permission from ref 37. Copyright 1967 Argonne National Laboratory.

By the end of the 1960s, Argonne had almost exclusively redirected their research toward high specific energy density lithium–chalcogenide cells for use in electric vehicles.[43–46,48,49,51–53,65] Not long after this, Argonne shifted direction again, this time toward Li–FeS cells, after the accidental discovery of FeS formation during the testing of Li–S cells in iron containers, which led to greatly enhanced cell cyclability.[66] As a result, the low specific energy density of bimetallic galvanic cells made them comparatively unattractive for portable applications and much of the aforementioned research fell into obscurity for the next few decades.

3. PRESENT WORK

This section aims to reintroduce liquid metal battery technology, provide insight into research challenges, and give perspective on where new opportunities lie. We endeavor to present researchers with a thorough introduction to the basic thermodynamics, economics, and unique properties of liquid metal battery systems.

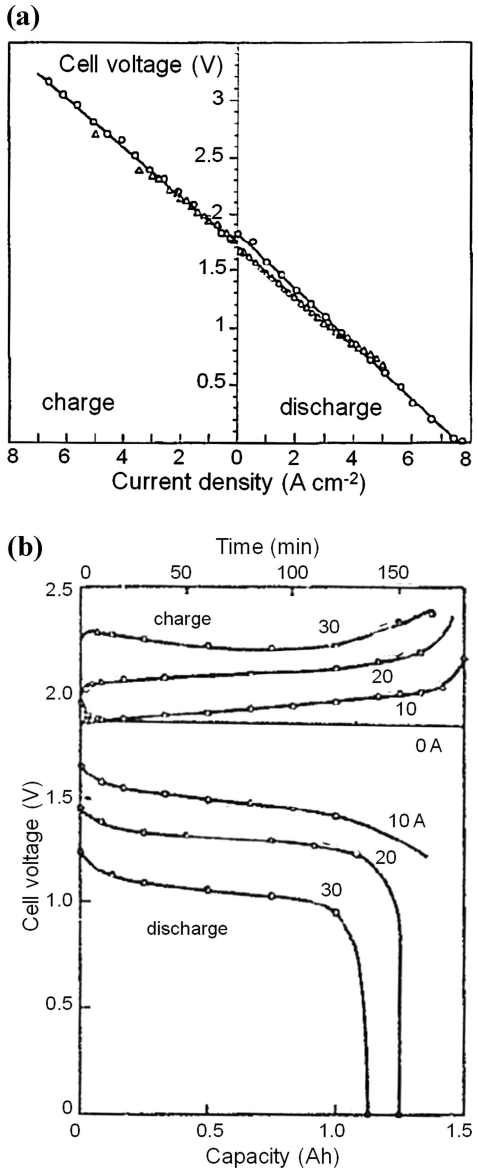

Figure 10. A Li|LiF–LiCl–Li|Te bimetallic secondary cell developed at Argonne National Laboratory: (a) plot of cell voltage as a function of steady-state current density at 470 °C, where circles (○) represent data for a cell with 9.6 Ah capacity, 3.9 cm^2 negative electrode area, 10 cm^2 positive electrode area, and 0.5 cm interelectrode distance and triangles (△) are for a cell with 1.6 Ah capacity, 10 cm^2 negative electrode area, 10 cm^2 positive electrode area, and 0.5 cm interelectrode distance; (b) plot of cell voltage versus capacity at various constant-current discharge rates and 480 °C with a 10 cm^2 electrode area and 0.5 cm interelectrode distance. Reprinted with permission from ref 37. Copyright 1967 Argonne National Laboratory.

3.1. Electrodes

Implicit in the design of any new battery system is the selection of which electrode chemistry to investigate in order to maximize performance and provide quantifiable benefits over existing technologies. Traditionally, metrics such as energy efficiency, energy density, and power density are employed to compare the relative strengths and weaknesses of electrochemical energy storage systems for a particular application. By contrast, grid-scale energy storage technologies are stationary, and therefore generally unconstrained by the need for high energy and power densities. Despite the presence of fewer

dx.doi.org/10.1021/cr300205k | Chem. Rev. 2013, 113, 2075–2099

Table 3. Equilibrium Cell Voltages from Full-Charge to Full-Discharge (V) of A–B Electrode Couples[a]

	A					
B	Li	Na	K	Mg	Ca	Ba
Zn	0.31–0.07[125]			0.21–0.08[74,83]	0.44–0.17[76,87]	
Cd	0.56–0.37[140b]	0.22–0.02[81,114]		0.21–0.09[71]		
Hg		0.67–0.13[75,82,84,103]	0.72–0.07[22,67]			
Al	0.30–0.30[92b]			0.20–0.07[77]	0.44–0.41[105]	0.53–0.15[122]
Ga	0.59–0.57[101b]	0.20–0.01[93,127]		0.25–0.14[73,79,94]		
In	0.55–0.50[97]	0.30–0.06[108,114]	0.24–0.02[123,136]	0.24–0.11[73,79]	0.62–0.34[88]	
Tl		0.42–0.11[98]	0.44–0.07[69]	0.23–0.12[72]		
Sn	0.70–0.57[99,100]	0.45–0.22[78,90,108,109,114]		0.35–0.19[85,112]	0.77–0.51[95]	1.08–0.71[95]
Pb	0.68–0.42[137]	0.47–0.20[86,111]	0.51–0.15[70,117]	0.21–0.13[79,112]	0.69–0.50[95]	1.02–0.66[95]
Sb	0.92–0.92[91]	0.86–0.61[80,116,128]	1.01–0.54[121,129]	0.51–0.39[85,112]	1.04–0.94[95]	1.40–1.15[95]
Bi	0.86–0.77[91]	0.74–0.47[37,113,116,126]	0.90–0.45[116,120]	0.38–0.27[85,112]	0.90–0.79[89,95,96]	1.30–0.97[95]
Te	1.76–1.70[42,134]	1.75–1.44[110]	2.10–1.47[119]			

[a]Equilibrium cell voltages as function of mole fraction, $E_{cell,eq}(x_A)$, are estimated from full-charge, $E_c(0.10, 0.05)$, to full-discharge, $E_d(0.50, 0.33)$, as discussed in the text. [b]Deviations from this calculation method: (1) Li–Al cells, $E_d(0.47)$; (2) Li–Ga cells, $E_d(0.45)$; (3) Li–Cd, $E_c(0.11)$ and $E_d(0.45)$.

constraints, stationary energy storage solutions must provide significant levels of energy or power, depending on the application, at particularly stringent price points. Thus, in identifying candidate systems, the complementary metrics of voltage (impacting rate capability and energy efficiency) and electrode material cost per unit of energy storage capacity ($\$ kWh^{-1}) are used to evaluate candidate electrode chemistries. In addition to metrics that directly quantify the cost and performance of the cell, electrode alloying is identified as a promising path forward to lower system-level costs by depressing the melting point and thus operating temperature of the battery.

3.1.1. Thermodynamics. The theoretical voltage of any electrochemical cell is determined by the fundamental thermodynamics of the negative and positive electrode materials. For liquid metal battery systems, there are over 100 possible binary alloy electrode combinations, each carrying with it a unique voltage discharge profile. The evaluation of the thermodynamic properties of binary alloy systems enables the identification of chemistries with higher cell voltages, which facilitate greater cell efficiencies at faster charge–discharge rates.

The generic liquid metal battery electrochemical cell can be written as

$$\mathrm{A(l)|AX}_z\mathrm{(l)|A(in\ B)} \tag{1}$$

where A is the negative electrode metal, B is the positive electrode metal, and AX_z is an alkali or alkaline-earth molten salt electrolyte. For this cell, the generic negative and positive half-cell reactions are

$$\text{negative} \qquad \mathrm{A(l)} = \mathrm{A}^{z+} + ze^-$$

$$\text{positive} \qquad \mathrm{A}^{z+} + ze^- = \mathrm{A(in\ B)} \tag{2}$$

and the overall cell reaction is

$$\text{cell} \qquad \mathrm{A(l)} = \mathrm{A(in\ B)} \tag{3}$$

The thermodynamic driving force is the change in partial molar Gibbs free energy,

$$\Delta\bar{G}_{cell} = \bar{G}_{A(in\ B)} - \bar{G}_{A(l)} \tag{4}$$

where the partial molar Gibbs energy $\bar{G}_i$ for each component i is given by

$$\bar{G}_{A(in\ B)} = G^\circ_{A(l)} + RT\ln a_{A(in\ B)}$$

$$\bar{G}_{A(l)} = G^\circ_{A(l)} + RT\ln a_{A(l)} \quad (a_{A(l)} = 1) \tag{5}$$

where a_i is the activity, $G^\circ_{A(l)}$ the standard chemical potential, R the gas constant, and T temperature. From the Nernst equation

$$\Delta\bar{G}_{cell} = -zFE_{cell,eq} \tag{6}$$

and eqs 4 and 5, the cell equilibrium voltage is related to the change in partial molar Gibbs free energy

$$E_{cell,eq} = -\Delta\bar{G}_{cell}/(zF) = -(RT/(zF))\ln a_{A(in\ B)} \tag{7}$$

where F is the Faraday constant and z the number of electrons. Conceptually, the thermodynamic driving force for cell discharge can be interpreted as emanating from a strong interaction of metal A with metal B, in which the activity of A can be extremely low ($a_{A(in\ B)}$ can be as low as 10^{-10}). This is manifest in the form of a high equilibrium cell voltage.

Experimental measurements of enthalpies of reaction, electromotive force, vapor pressure, and chemical equilibrium have been made to determine the thermodynamic activities of most binary alloys as a function of mole fraction and temperature [$a_A = f(x_A,T)$] and are readily available in the literature.[22,37,67−141] These data can be used to calculate the theoretical cell discharge profile of an electrode couple; however, a detailed comparison of the multitude of possible liquid metal battery electrode couples is impractical due to the wide variety of phase behavior exhibited in binary alloy systems. To address this issue, an imprecise, but effective method for estimating cell voltages for binary alloy electrode couples is constructed here. From literature data, the equilibrium cell voltages in Table 3 were calculated at two different mole fractions, x_A, corresponding roughly to the cell voltage at full-charge, E_c, and discharge, E_d. In order to avoid the steep rise in voltage as the positive electrode approaches infinite dilution ($x_A \to 0$), E_c is approximated from the theoretical voltage at full-charge mole fractions, $x_{A,c} = 0.10$ and 0.05 for alkali and alkaline-earth systems, respectively. The full-discharge voltage, E_d, is obtained from the theoretical cell voltage at discharge mole fractions, $x_{A,d} = 0.50$ and 0.33 for alkali and alkaline-earth systems, respectively, selected such that both systems have equivalent negative electrode molar capacities [i.e., $zn_A = n_B$, where for alkali systems $z = 1$, alkaline-earth systems $z = 2$, and

dx.doi.org/10.1021/cr300205k | Chem. Rev. 2013, 113, 2075–2099

$x_{A,d} = n_A/(n_A + n_B)$]. In most cases, the equilibrium cell voltages were estimated at temperatures slightly above the melting point of the higher melting electrode; however, it should be noted that the temperature dependence of the cell potential tends to be small (typically less than ±0.02 V/100 °C) over a wide range of concentrations.

The complexity of estimating a full theoretical discharge profile is illustrated by the Ca–Bi system presented in Figure 11.[141] Three distinct features can be observed in this discharge profile: (1) a sharp increase in cell voltage as the calcium approaches infinite dilution ($x_{Ca} \rightarrow 0$); (2) a cell voltage plateau corresponding to a two-phase liquid–solid region ($0.25 < x_{Ca} < 0.52$); and (3) a steep decrease in cell voltage to zero as the solid intermetallic species Ca_5Bi_3 is formed ($x_{Ca} > 0.63$). In Figure 11, the fully charged, E_c, and discharged, E_d, states are indicated, and from these values, the average equilibrium cell voltage, $\hat{E}_{cell,eq} = (E_c + E_d)/2$, is closely approximated. Despite the limitations of this approximation, this example demonstrates the utility of the approach. For comparison, the estimated fully charged and discharged equilibrium cell voltages of all known binary electrode couples are given in Table 3.

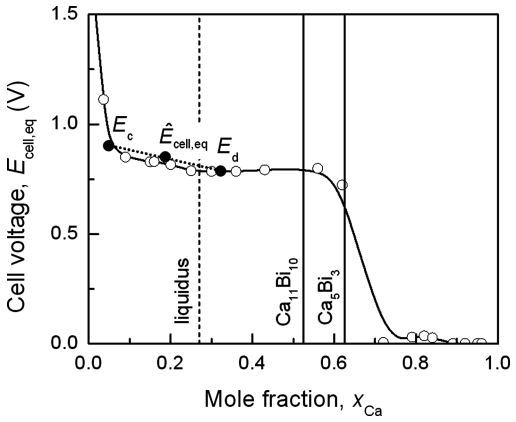

Figure 11. Plot of the measured equilibrium cell voltage as a function of calcium mole fraction of Ca(s)|CaF_2(s)|Ca(in Bi) cell at 600 °C. Reprinted with permission from ref 141. Copyright 2012 Elsevier.

3.1.2. Economics. Based upon the equilibrium cell voltages reported in Table 3, candidate electrode systems are compared on a cost per energy basis ($ kWh^{-1}), which uses 2010–2011 average monthly bulk metal market prices, $\hat{P}_i$, for each electrode material i, according to

$$\hat{P}_i = m^{-1} \sum_j^m \hat{P}_{i,j} \tag{8}$$

where $\hat{P}_{i,j}$ is the average price of month j and m is the number of months.[142] Due to the large volumes of metals that would be required for grid-scale energy storage applications, all prices used are from bulk quotations on the scale of metric tons at purities greater than 99%. In addition, because the prices of commodities change frequently and unpredictably, there are no fundamental limitations to cost metrics (i.e., they are derived from market prices) as there are with thermodynamic or performance metrics. Thus, when possible a ratio of the standard deviation in 2010–2011 monthly prices, $\hat{P}_{i,j}$, normalized by the monthly average price, $\hat{P}_i$, over that period is reported in order to quantify the recent volatility of the metal according to

$$\sigma_i = \hat{P}_i^{-1} \sqrt{(m-1)^{-1} \sum_j^m (\hat{P}_{i,j} - \hat{P}_i)^2} \times 100\% \tag{9}$$

The estimated cost of energy for electrode couples, C_E^{est}, on a per unit energy basis (in $ kWh^{-1}) is calculated from

$$C_E^{est} = (x_{A,d} z F \hat{E}_{cell,eq})^{-1} \sum_i x_i \hat{P}_i \tag{10}$$

where the average monthly bulk metal market prices, $\hat{P}_i$, are from Table 4, the average equilibrium cell voltages, $\hat{E}_{cell,eq}$, for each electrode couple are calculated from Table 3, $x_{A,d}$ represents the estimated negative electrode full-discharge composition, and x_i is the mole fraction of electrode component i in a cell. Implicit to this calculation are several simplifying assumptions: (1) cell charge–discharge energy efficiency is 100%; (2) cell discharge compositions $x_{A,d}$ are estimated to be 0.50 or 0.33 depending on the charge valence z of the active species; (3) electrode utilization is 100% such that the complete discharge of all active material is achieved; (4) the costs of the electrolyte and cell container are neglected; (5) the metal market prices are a fair approximation of costs for the required metal purity.

Table 4. Average Monthly Metal Prices $\hat{P}_i$ and Volatilities σ_i.[142]

metal, i	$\hat{P}_i$ ($ mol^{-1})	σ_i (%)
Li	0.43	2
Na[a]	0.057	
K[a]	5.1	
Mg[a]	0.069	
Ca[a]	0.14	
Ba[a]	0.82	
Zn	0.15	5
Cd	0.39	15
Hg	0.27	11
Al	0.066	6
Ga	51	19
In	74	19
Tl[a]	1200	
Sn	3.2	11
Pb	0.52	6
Sb	1.8	14
Bi	4.9	14
Te	44	22

[a]Prices are obtained from bulk quotations from the suppliers.

From these data, a few important trends emerge. First, the range in material prices spans 5 orders of magnitude, while cell voltage values vary by less than 1 order of magnitude, thus illustrating the importance of using a cost metric when selecting candidate electrode couples for grid-scale energy storage applications. Second, price fluctuations are much more pronounced for positive than for negative electrode materials, a behavior that suggests that future cost modeling of scale-up should factor in the variability of positive electrode prices, while negative electrode costs can be assumed to be constant. Lastly, from Table 5, it is evident that the high prices of some metals preclude their application in grid-scale energy storage. Whether due to low equilibrium cell voltages or high cost of electrode

dx.doi.org/10.1021/cr300205k | Chem. Rev. 2013, 113, 2075–2099

Table 5. Estimated Cost of Energy for A–B Electrode Couple Candidates ($ kWh^{-1})

	A					
B	Li	Na	K	Mg	Ca	Ba
Zn	110			26	26	
Cd	65	140		100		
Hg		31	510			
Al	61			27	12	52
Ga	3300	18000		9600		
In	5300	15000	23000	16000	5600	
Tl		170000	180000	250000		
Sn	210	370		440	190	150
Pb	64	64	630	120	36	40
Sb	89	93	330	150	69	64
Bi	240	300	550	560	220	170
Te	950	1000	1000			

couples, cells based on K, Ga, Ge, In, Tl, and Te are likely unsuitable for grid-scale liquid metal batteries.

The range of estimated costs including price volatility of promising electrode couples (C_E^{est} < $100 kWh^{-1}) from Table 5 are plotted in Figure 12. Some of the strengths and weaknesses

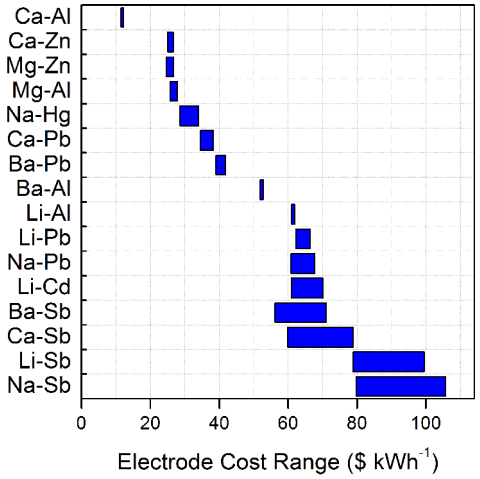

Figure 12. Plot of promising liquid metal battery electrode material energy costs (<$100 kWh^{-1}) incorporating the market price volatility of electrode materials.

of this evaluation are immediately apparent. For example, aluminum-based couples would appear to be the most attractive candidates based on cost, but most such cells exhibit average equilibrium voltages less than 0.50 V, too low to make them suitable for most battery applications. On the other hand, Sb-based couples appear favorable based on this analysis and have cell voltages typically above 0.70 V.

3.1.3. Alloying. In addition to electrode couple voltage and cost, the cell operating temperature is a key parameter for the practical operation of a liquid metal battery. The minimum cell operating temperature is determined by the melting point of the electrolyte and electrode materials. A reduced cell operating temperature decreases detrimental effects caused by corrosion and self-discharge, while simultaneously simplifying sealing and thermal management. In parallel, a lower operating temperature requires less in the way of Joule heating and is thus conducive to a higher round-trip storage efficiency (lower parasitic ohmic losses). By definition, a liquid metal battery must have liquid metal electrodes with distributed densities to ensure self-segregation of the three liquid layers. In Table 6, the liquid density, ρ_m, at the melting temperature, T_m, for each candidate electrode material is given.[143]

Table 6. Liquid Density, ρ_m, at Melting Temperature, T_m, of Candidate Electrode Materials[143]

electrode	ρ_m (g cm^{-3})	T_m (°C)
A		
Li	0.51	181
Na	0.93	98
K	0.83	63
Rb	1.46	39
Cs	1.84	28
Mg	1.58	650
Ca	1.38	842
Sr	2.38	777
Ba	3.34	727
B		
Zn	6.57	420
Cd	8.00	321
Hg	13.53	−39
Al	2.38	660
Ga	6.08	30
In	7.02	157
Tl	11.22	304
Sn	6.99	232
Pb	10.66	327
Sb	6.53	631
Bi	10.05	271
Te	5.70	450

The cost and voltage metrics in the previous sections assume that each electrode contains a pure metal. However, the use of pure metals is not mandatory, and liquid metal battery electrodes composed of alloys can have superior electrical performance and longer service lifetime enabled by a reduced cell operating temperature. In some cases, alloyed electrodes incur penalties such as a lower cell voltage, a decrease in rate capability, and a higher cell cost. Therefore, alloying liquid metal battery electrodes should aim to reduce the electrode melting temperature, while maintaining a low cost and high voltage.

3.1.3.1. Negative Electrodes. An alloy (A–A′) of the active component A in the negative electrode must also remain less dense than the electrolyte and only incorporate elements (A′) only more noble than component A to avoid reacting with the electrolyte. The Ca–Mg system for Ca-based cells is an example that meets these requirements. Calcium is an economically attractive negative electrode candidate with an undesirably high melting point (842 °C); however, a Ca–Mg alloy negative electrode can substantially reduce the electrode melting and cell operating temperatures (<600 °C), Figure 13a.[144] Since the concentration of component A (e.g., Ca) varies with the state-of-charge, the cell operating temperature must be safely above the eutectic temperature to ensure that the electrode remain liquid during operation. Moreover, in selecting the negative electrode alloy one must balance the negative impact of a reduced cell voltage with the positive impact of a suppressed metal solubility in the electrolyte

dx.doi.org/10.1021/cr300205k | Chem. Rev. 2013, 113, 2075–2099

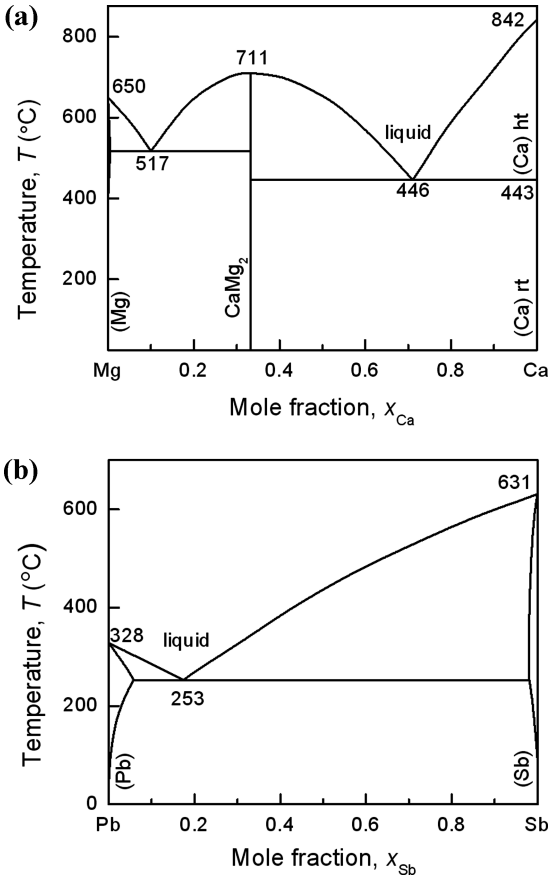

Figure 13. Binary phase diagrams of (a) Ca–Mg and (b) Pb–Sb systems. Reprinted with permission from ref 144. Copyright 2006 ASM International.

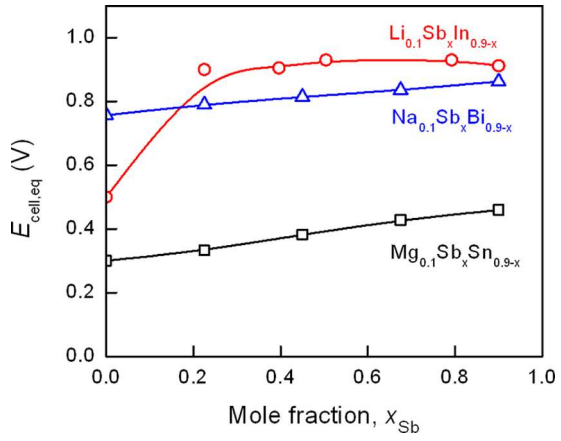

Figure 14. Plots of Al|A–B–B′ equilibrium cell voltages as a function of antimony mole fraction for ternary alloy systems (A–B–B′), where Li–Sb–In ternary alloys were measured for $Li_{0.1}In_{0.9}$ alloys at 360–415 °C,[91,99,145,146] Na–Sb–Bi ternary alloys for $Na_{0.1}Bi_{0.9}$ alloys at 577 °C,[128] and Mg–Sb–Sn ternary alloys for $Mg_{0.1}Sn_{0.9}$ alloys at 800 °C.[112]

(discussed in section 3.2), both of which result from a decrease in activity of A in the negative electrode.

3.1.3.2. Positive Electrodes. Alloying a positive electrode material (B) with a second component (B′) results in the formation of an A–B–B′ ternary alloy upon cell discharge. Binary systems of electropositive elements often exhibit deep eutectics, substantially reducing an electrode melting point, as in the Sb–Pb system depicted in Figure 13b.[144] Unfortunately, without detailed knowledge of the thermodynamics of the ternary system, there is no clear-cut way to evaluate the activity of A in B–B′ alloys and the resulting cell voltage. As illustrated in Figure 14, some ternary systems have a voltage that is proportionally dependent on B–B′ composition (e.g., Mg–Sb–Sn[112] and Na–Sb–Bi[128]), while other alloy systems exhibit cell voltages dominated by the more highly solvating binary system (e.g., Li–Sb–In[145,146]).

3.2. Electrolyte

The selection and properties of the molten salt electrolyte are critical to the performance of a liquid metal battery. The operation of candidate electrode couples in a rechargeable liquid metal battery cell requires suitable electrolytes with the desired characteristics: (1) low melting temperature; (2) minimal metal solubility; (3) no irreversible side reactions of spectator ions within the operating voltage window; (4) a density intermediate between the positive and negative electrodes to facilitate the self-segregation of the three liquid layers; (5) high ionic conductivity for high rate capability and energy efficiency. Of these, the solubility of metal in molten salt electrolytes presents perhaps the greatest challenge to liquid metal battery systems, because it leads to a high self-discharge current and low Coulombic efficiency.

Over the last century, the miscibility of liquid metals in halide salts has been of significant commercial interest for electrometallurgical processes, such as in the electrolytic production of aluminum. In a number of thermodynamic and electrical conductance studies, metals were found to form true metal–metal halide solutions.[147−150] While there is no consensus on the nature of this phenomenon, several mechanisms have been proposed. These include (1) the solvation of atoms that retain their individuality and are evenly distributed throughout the volume of the solution [e.g., Na(l) = Na(in NaCl)], (2) a chemical reaction between the electrolyte and the metal through the formation of ions or subions of lower valency such as Na_2^+ or Ca_2^{2+} [e.g., Na(l) + Na^+(in NaCl) = Na_2^+(in NaCl)], and (3) the ionization of the metal (e.g., Na = $Na^\bullet$ + e') combined with the formation of ionic vacancies (e.g., V_{NaCl} = V'_{Na} + $V^\bullet_{Cl}$) to create localized solvated electrons in anion vacancies (e.g., V_{NaCl} + Na = $Na^\times_{Na}$ + $e^\times_{Cl}$) analogous to F-center defects in ionic crystals.[148,151]

If one considers a simplified reaction for the dissolution of electrode metal A into a molten salt electrolyte,

$$\text{A(in electrode)} = \text{A(in electrolyte)} \tag{11}$$

then the equilibrium Gibbs free energy of reaction is

$$\Delta_r G^\circ = -RT\ln K_{eq} \tag{12}$$

where the equilibrium constant, K_{eq}, is given by the activity of metal A in the electrolyte $a_{A(\text{in electrolyte})}$ and the electrode $a_{A(\text{in electrode})}$,

$$K_{eq} = \frac{a_{A(\text{in electrolyte})}}{a_{A(\text{in electrode})}} \tag{13}$$

Based on this simple model, there are at least two possible approaches to thermodynamically limiting the solubility of metal A in the electrolyte: (1) reduce T (assuming $\Delta_r H^\circ > 0$), or (2) decrease $a_{A(\text{in electrode})}$. Perhaps the most effective of these is identifying low melting point electrolytes to reduce the cell operating temperature, since the equilibrium constant goes as

dx.doi.org/10.1021/cr300205k | Chem. Rev. 2013, 113, 2075−2099

the exponential of temperature, $K_{eq} = \exp(-\Delta_r G^\circ/(RT))$. The other approach requires decreasing the activity of metal A in the electrode through alloying the electrode with another metal, as discussed in section 3.1.3.

The solubilities of alkali and alkaline-earth metals in their respective halide salts are listed in Table 7, which shows that solubility generally increases with atomic number (Li < Na < K < Rb < Cs). Liquid cesium exhibits complete miscibility with molten cesium halides, while liquid lithium has the lowest solubility of all alkali metals. Similarly, liquid alkaline-earth metal solubility in alkaline-earth halide molten salts increases with increasing atomic number (Mg < Ca < Sr < Ba). For both alkali and alkaline-earth liquid metals, the solubility in their respective halide melts increases with the halide atomic number (F < Cl < Br < I). Finally, the solubility of a metal is observed to be at a maximum in a melt comprising only the cation of the metal; in contrast, a melt containing a plurality of cations will exhibit reduced metal solubility as well as offer the advantage of a lower melting temperature.[148,149,152−160] For example, Bukun and Ukshe[148] showed that for a given magnesium chloride concentration the solubility of magnesium metal decreases with decreasing polarizing power of the foreign cations (e.g., Ba, Ca, K, Na, Li), as shown in Table 8. Similarly, the solubility of liquid metals in molten salt electrolytes can be suppressed by alloying the liquid metal to decrease its activity. For example, Sharma[161] showed that calcium solubility in calcium chloride decreased from 2.1 to 0.3 mol % by alloying calcium with 70 mol % copper at 800 °C, as shown in Table 9.

Table 7. Solubility of Alkali and Alkaline-Earth Metals in Their Pure Molten Halide Salts

metal	halide salt	solubility (mol %)	temp (°C)
Li	LiF[149,158]	1.0	847
	LiCl[149,158]	0.5−2.0	640−1000
	LiI[149,158]	1.0−2.5	468−950
Na	NaF[149,153,155]	3.0	990
	NaCl[149,153,155]	2.1	795
	NaBr[149,153,155]	2.9	740
	NaI[149,153,155]	1.6	657
K	KF[149,152,154]	4.9	849
	KCl[149,154]	11	751
	KBr[149,154]	19	708
	KI[149,154]	14	658
Rb	RbF[149,156]	9.0	773
	RbCl[149,156]	18	696
	RbI[149,156]	22	615
Mg	$MgCl_2$[148,149]	0.20−1.2	714−900
	MgI_2[148]	1.3	900−1000
Ca	CaF_2[149,159]	26	1290
	$CaCl_2$[148,149,157]	2.7−5.7	820−1000
	$CaBr_2$[149]	2.3	827
	CaI_2[148,149]	3.8−9.6	831−1000
Sr	SrF_2[148]	20	1000
	$SrCl_2$[148,149,160]	5.5−25	839−1000
	$SrBr_2$[148,160]	21−35	900−1000
	SrI_2[148,160]	27−40	900−1000
Ba	BaF_2[148]	22	1050
	$BaCl_2$[148,149,160]	15−30	890−1050
	$BaBr_2$[148,160]	18−37	900−1050
	BaI_2[148,160]	39	1050

Table 8. Solubility and Polarizing Power of Magnesium in $MgCl_2$−ACl_z Molten Salts at 800 °C[148]

electrolyte (50−50 mol %)	Mg solubility (mol %)	polarizing power[a] (Å^{-2})
$MgCl_2$−$MgCl_2$	0.87	3.28
$MgCl_2$−$CaCl_2$	0.42	1.76
$MgCl_2$−LiCl	0.40	1.64
$MgCl_2$−SrCl	0.37	1.34
$MgCl_2$−$BaCl_2$	0.34	0.98
$MgCl_2$−NaCl	0.17	1.04
$MgCl_2$−KCl	0.15	0.56

[a]Defined as z/R^2, where R is the ionic radius of cation A^{z+}.

Table 9. Solubility of Calcium from Ca−Cu Alloys in $CaCl_2$ Molten Salt at 800 °C[161]

Ca−Cu alloy (mol %)	Ca solubility (mol %)
100−0	2.14
76−24	1.80
70−30	1.74
63−37	1.66
55−45	0.82
43−57	0.58
30−70	0.26

When one considers the use of foreign cations in molten salt electrolytes, special care must be taken to avoid irreversible reactions with the liquid metal electrodes. Even for reactions that exhibit positive Gibbs free energies ($\Delta_r G > 0$), sufficient equilibrium concentrations or current-induced deviations from equilibrium can cause irreversible side reactions, that is, metathesis. For example, Seefurth and Sharma[162] showed that when lithium metal contacts LiCl−KCl eutectic melt at 375−500 °C, lithium is lost through a reaction with potassium chloride to form lithium chloride and liquid potassium

$$\mathrm{Li(l) + KCl(l) \rightarrow LiCl(l) + K(l)} \quad (14)$$

followed by potassium evaporation

$$\mathrm{K(l) \rightarrow K(g)} \quad (15)$$

As a consequence, all-lithium cation electrolytes are usually selected for use with pure lithium in high temperature molten salt electrochemical systems.

In order to preserve the self-segregating properties of the liquid metal battery, the density of the electrolyte must be appropriately designed to lie between the densities of the negative and positive electrodes. In Table 10, the melting temperatures and densities of alkali and alkaline-earth halide molten salts are given.[143] From these values, the density of a molten salt electrolyte solution, comprised of individual metal halide salt components i with density ρ_i and mass fraction w_i can be approximated by

$$\rho = \left(\sum_i (w_i/\rho_i)\right)^{-1} \quad (16)$$

Another important electrolyte parameter for battery cell operation is the decomposition potential of the molten salt electrolyte [$2AX_z(l) \rightarrow 2A + zX_2(g)$], which will limit the maximum charge voltage of the cell. Decomposition potentials for pure metal halide salts are listed in Table 11.[163]

Over the last several decades, specific multicomponent (binary, ternary, and quaternary) metal halide molten salts

dx.doi.org/10.1021/cr300205k | Chem. Rev. 2013, 113, 2075−2099

Table 10. Melting Temperature (T_m) and Liquid Density (ρ) at Melting Point of Pure AX_z Halide Salts[143]

	X⁻							
	F⁻		Cl⁻		Br⁻		I⁻	
A^{z+}	T_m (°C)	ρ (g cm^{-3})	T_m (°C)	ρ (g cm^{-3})	T_m (°C)	ρ (g cm^{-3})	T_m (°C)	ρ (g cm^{-3})
Li^+	848	1.81	610	1.50	552	2.53	469	3.11
Na^+	996	1.95	801	1.56	747	2.34	660	2.74
K^+	858	1.91	771	1.54	734	2.13	681	2.45
Rb^+	833	2.87	715	2.25	682	2.72	642	2.90
Cs^+	703	3.65	645	2.79	636	3.13	621	3.20
Mg^{2+}	1263		714	1.68	711	2.62	634	3.05
Ca^{2+}	1418	2.52	775	2.09	742	3.11	783	3.44
Sr^{2+}	1477	3.47	874	2.73	657	3.70	538	4.09
Ba^{2+}	1368	4.14	962	3.17	857	3.99	711	4.26

Table 11. Decomposition Potentials (V) of Pure AX_z Halide Salt at 700 °C[163]

	X⁻		
A^{z+}	Cl⁻	Br⁻	I⁻
Li^+	3.41	3.03	2.56
Na^+	3.39	2.98	2.42
K^+	3.53	3.16	2.59
Rb^+	3.62	2.73	2.25
Cs^+	3.68		2.40
Mg^{2+}	2.61	2.21	1.62
Ca^{2+}	3.38	2.88	2.24
Sr^{2+}	3.54	3.04	2.55
Ba^{2+}	3.62	3.25	

have gained preference for a given active electrode species based upon melting temperature, conductivity, and minimal side-reactions. The most common multicomponent molten salt electrolytes used for Li-,[164−166] Na-,[37] Mg-,[57] and Ca-based[57−59] systems and their properties are given in Table 12.

3.3. Cell Performance

Since 2006, the development of liquid metal battery technology has been reinitiated by the authors at the Massachusetts Institute of Technology (MIT). Following the work carried out at Argonne National Laboratory in the 1960s, the more recent MIT investigations began with Na−Bi, but quickly migrated toward Mg−Sb and Li−Pb−Sb chemistries, which exhibit superior Coulombic efficiencies and are lower cost.

The construction and testing of liquid metal batteries requires special treatment of a couple of key components. First, it is often necessary to pretreat negative current collectors by immersing in a bath of the negative electrode liquid metal to ensure proper wetting and contact. Bader and Bussea[167] demonstrated that excellent wetting of sodium can be achieved with most metals after pretreating the metal in liquid sodium at 500−700 °C for several hours. Second, great care must be taken to minimize the exposure of active cell components to the ambient atmosphere due to the hygroscopic nature of most metal halide salts which leads to oxy-chloride formation and poor cell performance. To accomplish this, ultradry salts should be used, cells assembled in an ultradry, low oxygen concentration (<0.3 ppm) argon atmosphere glovebox, and tests carried out in hermetically sealed cells or in a glovebox fitted with furnace wells.

At MIT, a 1 Ah nominal capacity cell, depicted in Figure 15a, served as the test vehicle for exploring various chemistries, that is, electrodes and electrolyte. This design features a cell container that dually serves as the positive current collector, a negative current collector immersed in the negative liquid metal electrode, and an insulating sheath usually composed of high-purity hot-pressed boron nitride due to its chemical inertness and machinability. Because the 1 Ah cells are tested in an inert atmosphere glovebox, they are not sealed. While this is useful for rapid screening of new chemistries, it precludes the evaluation of metrics such as cell cycle life due to the gradual evaporation of active cell components. To address issues of sealing, thermal management, and battery cycle life, a 20 Ah sealed cell was also designed, constructed, and tested. This cell design features insulated electrical feedthroughs from the hot cell to an external cold zone, where an elastomer O-ring provides an airtight seal, as depicted in Figure 15b.

3.3.1. Na−Bi Cells. Sodium−bismuth liquid metal battery cells were tested using a NaF−NaCl−NaI eutectic salt at 560 °C, and key results are given in Table 13. Consistent with results obtained by Argonne National Laboratory, these cells achieved Coulombic and voltage efficiencies of 80% and 60%, respectively.

The realized electrode materials cost per unit energy, C_E^{real}, for Na−Bi cells was calculated from

$$C_E^{real} = (Q_d \hat{E}_{cell})^{-1} \sum_i x_i \hat{P}_i \quad (17)$$

where Q_d is the measured discharge capacity and $\hat{E}_{cell}$ is the average discharge cell voltage. For Na−Bi cells, the estimated

Table 12. Properties of Common Low Melting Molten Halide Salt Electrolyte Systems

cation	electrolyte	composition, mol %	T_m, °C	$\rho(T_0)$, g cm^{-3}	$\sigma(T_0)$, S cm^{-1}	T_0, °C
Li^+	LiCl−KCl[164]	41:59	353	1.63	1.7	476
	LiF−LiCl−LiI[165]	20:50:30	430			
	LiCl−LiI[166]	35:65	368	2.57	3.5	450
Na^+	NaF−NaCl−NaI[37]	15:16:53	530	2.54	1.7−2.0	560
Mg^{2+}	NaCl−KCl−$MgCl_2$[57]	30:20:50	396			
Ca^{2+}	LiCl−NaCl−$CaCl_2$−$BaCl_2$[57−59]	29:20:35:16	390	2.28	1.9	527

dx.doi.org/10.1021/cr300205k | Chem. Rev. 2013, 113, 2075−2099

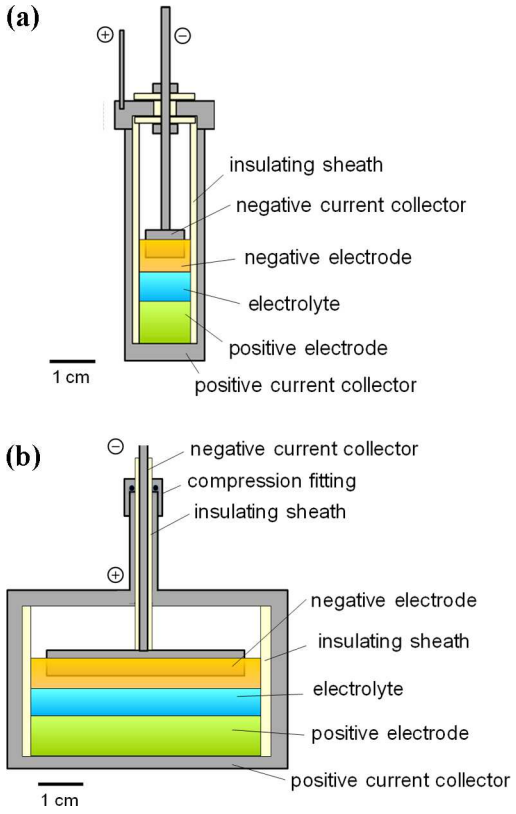

Figure 15. Schematics diagrams of nominal (a) 1 Ah capacity unsealed and (b) 20 Ah capacity sealed liquid metal battery cell designs for testing.

Table 13. Performance Characteristics of Liquid Metal Battery Chemistries

	unit	Na–Bi	Mg–Sb[168]	Li–Pb–Sb
electrode composition	mol %	39–61	30–70	45–38–17
electrolyte chemistry		NaF–NaCl–NaI	$MgCl_2$–NaCl–KCl	LiF–LiCl–LiI
electrolyte composition	mol %	15:32:53	50:30:20	20:50:30
operating temperature	°C	560	700	450
electrode area	cm^2	2.1	2.0	1.3
interelectrode distance	cm	1.0	1.0	1.0
charge–discharge current	A	0.53	0.10	0.34
theoretical capacity	Ah	1.00	3.2	0.77
discharge capacity	Ah	0.77	3.2	0.58
Coulombic efficiency	%	82	94	98
average discharge voltage	V	0.48	0.35	0.66
voltage efficiency	%	59	73	67
estimated electrode cost	$ kWh^{-1}	470	170	62[a]
realized electrode cost	$ kWh^{-1}	770	230	84

[a]Estimated electrode cost based upon Li–Sb binary system, assuming $\hat{E}_{cell,eq}$ = 0.92 V, x_{Li} = 0.45.

and realized costs of electrode materials were \$470 kWh^{-1} and \$770 kWh^{-1}, respectively. The discrepancy between these costs is the result of high current density operation imposed by the need to overcome the high self-discharge rate (~20 mA cm^{-2} at full-charge) caused by sodium solubility in the molten salt electrolyte. Ultimately, the work on Na–Bi cells was discontinued because of the high self-discharge rate and the high cost of bismuth.

3.3.2. Mg–Sb Cells. The high self-discharge current in Na-based cells motivated the investigation of Mg-based systems because of the extremely low solubility of magnesium in molten salt electrolytes compared with other alkali or alkaline-earth metals, as shown in Tables 7 and 8. Furthermore, antimony was selected for the positive electrode over bismuth because of its lower cost (\$1.8 mol^{-1} versus \$4.9 mol^{-1}, Table 4) and higher anticipated discharge voltage (0.45 V versus 0.30 V, Table 3). Based upon these factors, Mg–Sb cells incorporating a molten NaCl–KCl–$MgCl_2$ electrolyte were tested at 700 °C;[168] the key results are presented in Table 13.

As expected, Mg–Sb cells exhibited high Coulombic efficiency (over 94%); however, low voltage efficiencies were also observed (~73% at 50 mA cm^{-2}) as a consequence of relatively low electrolyte conductivity (~0.8 S cm^{-1}). The estimated and realized Mg–Sb electrode materials costs from this work were \$170 kWh^{-1} and \$230 kWh^{-1}, respectively (Table 13). On the basis of this cost (>\$100 kWh^{-1}), the low cell voltage, and limited rate capability, Mg–Sb cells were judged to be impractical for commercial applications.

3.3.3. Li–Pb–Sb Cells. After magnesium, lithium is the least soluble alkali or alkaline-earth metal in molten salts (Table 7). However, in contrast to magnesium-based melts, lithium halides have extremely high ionic conductivities (1.7–3.5 S cm^{-1}) and relatively low melting points (350–430 °C), see Table 12. Hence, combining a lithium negative electrode and a lithium halide electrolyte with an antimony positive electrode would make an attractive liquid metal battery with appealing values of estimated cost (\$89 kWh^{-1}, Table 5) and cell voltage (0.92 V, Table 3). Despite these attractive properties, the melting temperature of antimony (631 °C) restricts the operation of a Li–Sb cell to high temperatures, which leads to increased corrosion and self-discharge rates and complicates sealing and thermal management.

As presented in section 3.1.3, the melting temperature of an antimony-based positive electrode can be decreased by alloying. For this, an element is sought that has lower cost and melting temperature, for example, Zn, Cd, Hg, and Pb. Other elements, such as Sn and Bi meet the physical criteria but are too expensive (see Table 4).

Of the possible candidate alloys, a near-eutectic 30:70 mol % Sb–Pb alloy ($T_{liquidus}$ ≈ 330 °C) was selected for the positive electrode, Figure 13b. From the Li–Sb binary phase diagram[144] and the work of Weppner and Huggins,[91] only one high melting temperature intermetallic phase is expected to significantly reduce the cell voltage upon cell discharge, Li_3Sb (T_m = 1150 °C). Therefore, the target lithium concentration should be less than 75:25 mol % Li–Sb to yield a fully discharged cell composition of 45:38:17 mol % Li–Pb–Sb. On the preliminary assumption that the average equilibrium cell voltage for Li–Pb–Sb is similar to that of a Li–Sb ($\hat{E}_{cell,eq}$ = 0.92 V), the estimated electrode cost is \$62 kWh^{-1}.

With a theoretical capacity of 0.8 Ah and a full-discharge composition of 45:38:17 mol % Li–Pb–Sb, cells containing an electrolyte of LiF–LiCl–LiI eutectic (T_m = 430 °C) were constructed and tested at 450 °C. The results are given in Table 13. The Li–Pb–Sb cells achieved impressive 98% Coulombic and 67% voltage efficiencies at charge–discharge

dx.doi.org/10.1021/cr300205k | Chem. Rev. 2013, 113, 2075–2099

current densities of 280 mA cm^{-2}. Based upon the measured discharge capacity and voltage, a low realized electrode cost of \$84 kWh^{-1} was projected. Discrepancies between the estimated and realized electrode costs can be explained by (1) a lower than anticipated average cell equilibrium voltage (0.84 V as opposed to 0.92 V), (2) a lower discharge voltage due to current density dependent ohmic losses, and (3) poor electrode utilization (~75 mol % Li). These cells were charged−discharged for several hundred cycles; however, the characterization of long-term cycle life requires the development of seals to prevent electrolyte evaporation and needs further evaluation.

The ability to operate at high rates (current densities) is a potentially attractive attribute of liquid metal batteries for dual-purpose (high power and energy) applications. To this end, the rate capability of Li−Pb−Sb cells was evaluated upon charge and discharge at current densities of 0.14, 0.28, 0.55, and 1.1 A cm^{-2}. As evident from the results presented in Figure 16a, these cells can operate at current densities as high as 1.1 A cm^{-2}; however, at this high discharge rate there is a 40% loss in capacity. Moreover, even at relatively modest current densities of 0.14 A cm^{-2}, the discharge capacity falls well short of the theoretical capacity (80%). Based on the data presented in Figure 16a, we speculate that mass transport of lithium to and from the antimony electrode−electrolyte interface limits the discharge capacity.

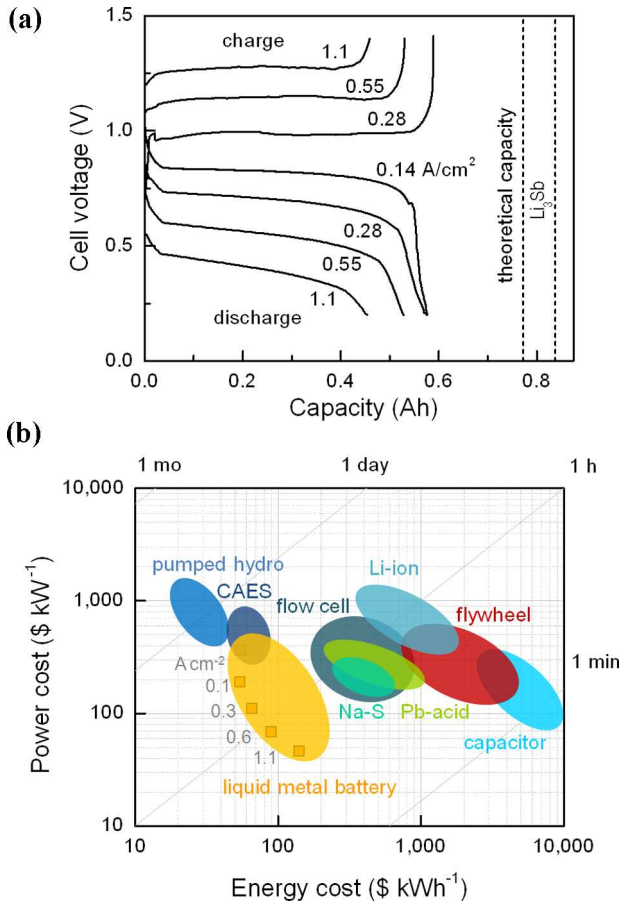

Figure 16. (a) Plot of cell voltage versus capacity upon charge and discharge at different current densities of a LiLiF−LiCl−LiI|Pb−Sb cell at 450 °C with 0.77 Ah theoretical capacity, 2.0 cm^2 electrode area, and 1.0 cm interelectrode distance. (b) Cost of energy versus power plot indicating various energy storage technologies (adapted from refs 8−10), where the real electrode materials costs measured for Li−Pb−Sb liquid metal battery cell are indicated by orange squares (■) and calculated from $C_E^{real} = (Q_d\hat{E}_{cell})^{-1}\sum_i x_i\hat{P}_i$ for cost of energy and $C_P^{real} = (I_d\hat{E}_{cell})^{-1}\sum_i x_i\hat{P}_i$ for cost of power at measured discharge current, I_d.

In Figure 16b, the realized electrode materials energy and power costs from the rate capability tests of the Li−Pb−Sb liquid metal battery cell are plotted, where the power costs are calculated from

$$C_P^{real} = (I_d\hat{E}_{cell})^{-1}\sum_i x_i\hat{P}_i \quad (18)$$

where I_d is the applied discharge current. Based on these data, the electrode material energy and power costs are estimated to be under \$100 kWh^{-1} and \$100 kW^{-1}, respectively. Assuming that the electrode materials comprise only about one-fourth of the cost of a battery system, the economics of the liquid metal battery appear promising for combining energy and power applications when compared with other existing energy storage technologies.

4. FUTURE WORK

Future research and development of liquid metal battery technology offers an exciting opportunity to explore rich, new battery chemistries. The development of a commercially viable liquid metal battery technology also presents enormous challenges, particularly with respect to demonstrating the long-term performance that this technology promises. Major obstacles to demonstrating long-life liquid metal batteries center on (1) the identification and verification of corrosion resistant cell components, (2) the engineering of robust, high temperature, insulating seals, (3) the development of efficient thermal management systems, and (4) the significant investment of time and resources necessary for demonstration.

4.1. New Chemistries

The wide-range of applicable chemistries makes liquid metal batteries a rich and promising avenue for future research and development. The analysis of thermodynamic cell potentials and estimated energy cost of binary electrode couples in the previous sections yielded 10 promising couples for liquid metal battery applications, that is, couples with average cell voltages over 0.4 V and estimated energy cost under \$100 kWh^{-1}, Table 14. The Li−Sb system investigated at MIT represents only one of these chemistries, but also illustrates how each new chemistry represents a unique set of challenges.

4.1.1. Lithium. Lithium is one of the most-widely studied negative electrode materials for electrochemical energy storage due to its high voltage capability, high specific and volumetric energy density, and facile transport properties. Beyond the Li−Sb system mentioned earlier, Li−Pb and Li−Cd chemistries also offer attractive economics; however, the development of these couples will demand cell operation at low current densities or the development of ultrathin electrolytes to minimize voltage inefficiencies and maximize energy efficiency.

4.1.2. Sodium. Promising sodium chemistries, such as Na−Hg and Na−Sb offer attractive economics. The primary challenge with sodium-based systems is the high solubility of sodium in molten salt electrolytes that endows the electrolyte with electronic conductivity and high self-discharge current, leading to low Coulombic efficiencies. The development of sodium-based chemistries will inevitably require the development of an electrolyte that minimizes sodium solubility.

dx.doi.org/10.1021/cr300205k | Chem. Rev. 2013, 113, 2075−2099

Table 14. Promising Liquid Metal Battery Electrode Couples, Estimated Costs, Cell Voltages, And Challenges

A–B	C^{est}_{A-B} ($ kWh^{-1})	$\hat{E}_{cell,eq}$ (V)	major challenges
Li–Cd	66	0.47	low voltage
Li–Pb	64	0.55	low voltage
Li–Sb	89	0.92	high T_m(Sb)
Na–Hg	31	0.40	solubility of Na, low voltage
Na–Sb	93	0.74	solubility of Na, high T_m(Sb)
Ca–Al	12	0.43	solubility of Ca, high T_m(Ca and Al), low voltage
Ca–Pb	36	0.60	solubility of Ca, high T_m(Ca)
Ca–Sb	69	0.99	solubility of Ca, high T_m(Ca and Sb)
Ba–Pb	40	0.84	solubility of Ba, high T_m(Ba)
Ba–Sb	64	1.28	solubility of Ba, high T_m(Ba and Sb)

4.1.3. Calcium. From 1950 to 1980, calcium negative electrodes were utilized in thermal batteries (Ca–$K_2Cr_2O_7$, Ca–$CaCr_2O_7$, and Ca–WO_3 cells) as a primary reserve battery for military applications.[169−171] These batteries exhibit high open-circuit voltages (2.4–3.3 V) and a complex series of irreversible electrochemical reactions.[171] For application in rechargeable liquid metal batteries, the high melting temperature (842 °C), reactivity, and solubility in molten salt electrolytes of elemental calcium present major challenges. As mentioned in section 3.1.3, the melting temperature of a calcium-based negative electrode can be reduced by alloying with more noble elements; however, this forfeits some electrode potential. The most promising calcium-based chemistries for liquid metal battery applications include Ca–Al, Ca–Pb, and Ca–Sb. The low cell voltage of Ca–Al and Ca–Pb combined with the common challenge of developing a compatible electrolyte leaves Ca–Sb as the leading calcium-based couple for liquid metal batteries.

4.1.4. Barium. Barium-based electrode couples have the highest average cell voltages of any liquid metal battery system and the low-cost barium chemistries include Ba–Pb and Ba–Sb couples. Unfortunately, barium-based chemistries are the least well characterized, and there are few data on barium-conducting molten salts. However, from what is known, the high solubility of barium in molten salts (Table 7) is expected to be a major challenge for developing barium-based liquid metal battery systems.

4.1.5. Strontium. The least amount of thermodynamic and economic data exist for strontium-based electrode couples, and therefore they are not covered in this review. Based upon the relatively high voltage observed in calcium- and barium-based systems, one might expect strontium-based electrode couples to exhibit similarly high cell voltages. However, strontium-based liquid metal batteries are also likely to be challenged by high metal solubility in the molten salt electrolyte.

4.2. Corrosion

In conventional batteries, the microstructural degradation of highly engineered solid-state electrodes is a key factor in limiting battery cycle life. By contrast, all-liquid electrodes in liquid metal batteries are inherently immune to microstructural degradation, thus enabling the potential for extraordinarily long cycle life. Hoopes cells for the electrolytic production of high-purity aluminum have operated continuously for more than 20 years, lending credence to the expectation that liquid metal batteries can exhibit long service lifetimes.[16] Despite advantages conferred by the liquid state, the high operating temperature and high reactivity of the electrodes of a liquid metal battery make corrosion of cell construction materials (current collectors, container, insulators, and seal) a primary concern for long-term performance.[63] Corrosion-resistant cell construction materials are required to maintain the mechanical and chemical integrity in order to prevent increased cell resistance and reduced cell capacity over time.

Corrosion of cell components is a complex phenomenon influenced by the combination of operating temperature and environment. Knowledge of in situ behavior of cell components is required in order to take into account the effects of any corrosion products that result from both chemical and electrochemical processes operative within the device. Corrosion-resistant, chemically compatible materials with various liquid metal battery negative electrodes, positive electrodes, and molten salt electrolytes identified in previous work are reported in Table 15.

Table 15. Candidate Corrosion Resistant Engineering Materials for Use with Liquid Metal Batteries

component	ferrous alloys	T_{max}[a] (°C)	refractory and non-metals	T_{max}[a] (°C)
Negative				
Na[37,173]	pure iron, ferritic/austenitic stainless steels	800	W, Ta, Mo	800
Li[37,173]	pure iron	800	W, Ta, Mo	800
	ferritic stainless steel	600		
Mg[144]	cast iron, low-carbon steel, high-chrome stainless steel	800	W, Ta, Mo	
Ca[88,144,175]	pure iron, low-carbon steel		W, Mo	
Electrolyte				
NaX[37,176]	austenitic stainless steels	700		
Positive				
Bi, Pb[173,177]	pure iron, low-carbon steel, ferritic/austenitic stainless	600	W, Mo, Nb, Ta	800
Sn[173,177]			W, Mo, Nb, Ta	800
Sb[144,173]			W, graphite	

[a]Maximum temperature, T_{max}, at which the corrosion resistance was evaluated.

4.2.1. Negative Current Collector. Negative current collector materials must possess the following attributes: high electronic conductivity, low cost, and high corrosion resistance to negative electrode metals, such as Li, Na, and K, which were extensively investigated as heat-transfer fluids for nuclear power generation systems.[172] A wide-range of engineering materials, including stainless steels and low carbon steels, were identified as being compatible with molten alkali metals.[173] Impurities such as oxygen and nitrogen were found to enhance corrosion;

dx.doi.org/10.1021/cr300205k | Chem. Rev. 2013, 113, 2075–2099

hence, their presence should be minimized.[37,172,174] While no explicit corrosion data have been collected for alkaline-earth metals, their immiscibility with pure iron and refractory metals[88,144,175] suggests that materials solutions for the negative current collector exist. In addition to direct contact with the negative electrode, the negative current collector must also be chemically compatible with the electrolyte and specifically evaluated for each chemistry.[176,177]

4.2.2. Positive Current Collector. The selection of a positive current collector material that is compatible with positive electrode metals such as Bi, Pb, Sn, and Sb can be a significant challenge due to their high dissolving power. Corrosion in molten heavy metals generally depends on the rate of dissolution and the solubility limit of the solid component material in the liquid metal. Side reactions that lead to the formation of surface intermetallic compounds or oxide films can influence corrosion rate and electrode stability. At typical liquid metal battery operating temperatures (400−700 °C), ferrous alloys were found to be corrosion resistant to molten Bi and Pb and therefore attractive candidates for positive current collectors.[37,173,177] Liquid antimony represents a unique challenge in that it alloys with almost every known metal. Based upon binary phase diagrams, only tungsten and graphite are known to be immiscible in molten antimony.

4.2.3. Electrical Insulator. In the construction of a cell, at least one dielectric break is needed to insulate the negative electrode from the positive electrode and to provide a hermetic seal. Insulating cell components include seals, sheaths, and electrolyte fillers for paste electrolytes. Compatibility requirements include corrosion resistance against molten salt electrolytes as well as negative electrode metals and their alloys. Insulating materials BN, Al_2O_3, and BeO were shown to be resistant to corrosion in the presence of molten sodium and Na−Pb, Na−Bi, and Na−Sn alloys and for molten lithium chemically compatible insulator materials include BeO, $Y_3Al_5O_{12}$, ThO_2, $CaZrO_3$, Y_2O_3, $MgAl_2O_4$, and AlN.[46,48] Very little work has been done on chemically compatible insulating materials for use with molten alkaline-earth metals. The issue remains of how to satisfy performance requirements at an acceptable cost.

4.3. Seals

A hermetic seal assumes a key role in the development of long-life liquid metal batteries by preventing detrimental secondary reactions and minimizing corrosion that can be caused by the ingress of oxygen, nitrogen, and moisture from the ambient atmosphere. The seal needs to be gastight, electrically insulating, chemically stable, and thermomechanically robust. The engineering of a seal is particularly challenging for high temperature battery applications due to the requirement for electrical insulation that necessitates the joining of dissimilar materials with vastly different coefficients of thermal expansion.

Seals can be broadly classified into two types: compressive and adhesive. A compressive seal fills the space between two or more mating surfaces to prevent leakage through the joined objects while placed under a mechanical load. An adhesive seal joins two materials by intermolecular forces that can be broadly categorized into dispersive, chemical, and diffusive bonding.

4.3.1. Compressive Seals. Metal/metal compressive seals are effective high temperature seals; however, this approach cannot be used for liquid metal batteries because they require an electrically insulating seal. Compressive elastomeric gaskets and O-ring seals are employed for moderate temperature applications up to ∼200 °C and can be used for higher temperature applications by positioning the sealing region away from the hot zone.[178] This approach was successfully employed at Argonne and MIT to demonstrate the performance of sealed liquid metal battery cells (see Figures 9a and 15b). While suitable for laboratory testing, elastomeric seals may be questioned for their long-term durability and high thermal losses that result in a low overall battery energy efficiency.

4.3.2. Adhesive Seals. For high temperature applications, glass/metal adhesive seals that form dispersive bonds are commonplace. However, dispersive bonds tend to be weak, and thus the thermal expansion coefficient of the seal must be carefully engineered to match the joining materials. By contrast, chemical and diffusion bonds have the potential to form stronger, more robust insulating seals and therefore are more promising for liquid metal battery applications.

Other high temperature battery systems, such as Na−S and Na−$NiCl_2$ (ZEBRA) utilize a diffusion-bonded adhesive-type seal that boast a calendar life of over 15 years.[179−181] Over the course of Na−S battery development, compressive and dispersive-bonded adhesive seals were investigated;[63] however, more robust diffusion-bonded seals were ultimately adopted. These seals are formed by subjecting an aluminum layer on an alumina substrate to high pressure and heat that promotes atomic interdiffusion.[182]

During the development of another high temperature battery system, Li−FeS batteries, a variety of glass seals was investigated. Unfortunately, commercially available silica-based materials were found to be chemically incompatible with lithium.[183] Later, a family of chalcogenide sealants (e.g., $CaAl_2S_4$) was developed to form chemically bonded seals with metals and ceramics, while exhibiting excellent chemical stability with Li and FeS reactants. Moreover, these chemistries were found to form high-strength seals and have compositions that could be varied to match thermal expansion coefficients ($(7−15) \times 10^{-6}$ K^{-1}) over a range of substrates.[169,183−185] These seals have demonstrated stability in Li−FeS batteries operated for 500 cycles and 2500 h[183] but are known to exhibit some degradation in the presence of moisture.[186]

Long-life, high-energy efficiency liquid metal batteries will inevitably require the development of robust, high-temperature insulating seals. Moreover, the development of a seal for liquid metal batteries will be unique for each battery chemistry. For Li−Sb−Pb liquid metal battery cells, the development of chalcogenide-based chemically bonded adhesive-type seals provides a promising direction.

4.4. Thermal Management

Liquid metal batteries have two features that make the engineering of their thermal management systems distinct: (1) elevated operating temperatures (typically >200 °C) that allow for efficient cooling and (2) thermal tolerance to wide-temperature swings (ΔT > 100 °C) with minimal loss in performance. One disadvantage of high temperature operation is that it requires the battery employ a hot seal to attain reasonable energy efficiencies.

Thermal management is critical to the successful operation of any battery technology.[63,169,187] The rate of heat generation, $\dot{Q}$, in a battery is a function of the current $I = zF\dot{n}_A$, where $\dot{n}_A$ is the oxidation or reduction rate of reactant A (mol s^{-1}). The rate of reversible entropic heat absorbed or generated (depending on whether $\Delta\overline{S} > 0$ or $\Delta\overline{S} < 0$) during the charge−discharge of a battery is given by

dx.doi.org/10.1021/cr300205k | Chem. Rev. 2013, 113, 2075−2099

$$\dot{Q}_{rev} = \dot{n}_A(-T\Delta\bar{S}_{cell}) \quad (19)$$

where from the thermodynamic relation $\Delta\bar{G} = \Delta\bar{H} - T\Delta\bar{S}$, the Nernst equation, and the definition of thermoneutral potential $E_{th} \equiv \Delta\bar{H}_{cell}/(zF)$, the reversible entropic heat generation or absorption rate is given by

$$\dot{Q}_{rev} = -I(E_{cell,eq} - E_{th}) \quad (20)$$

Assuming no Coulombic losses, the irreversible heat (Joule heating) generated during charge−discharge is a function of the current density dependent cell voltage inefficiencies described in section 1.2,

$$\dot{Q}_{irr} = |I| \sum_i \eta_i \quad (21)$$

and finally the total rate of heat generation upon charge and discharge is

$$\dot{Q}_{gen} = \dot{Q}_{rev} + \dot{Q}_{irr} \quad (22)$$

For optimal battery operation and high energy efficiency, the heat generated by cell charging and discharging should be carefully balanced with heat loss to the environment ($\dot{Q}_{loss} \approx \dot{Q}_{gen}$), where heat loss can take the form of conductive, convective, or radiative heat transfer. Ultimately, the degree of insulation or design of a cooling system will depend upon how the battery is operated.

5. CONCLUSIONS

Because liquid metals and molten salts present no major challenges in terms of materials expenses or fabrication costs, the development and design of liquid metal batteries can be constantly guided by a market price point instead of relying upon economies of scale to reduce costs. Such clarity in materials input costs allows technologists to employ the evaluative metric of cost per unit energy ($ kWh^{-1}) at each decision point along the path toward commercialization. Moreover, by circumventing the electrode solid-state decay and dendritic growth mechanisms that limit the life of traditional batteries, liquid metal batteries have the potential for unprecedented operational life, which makes them economically attractive for grid-level energy storage when amortized over their cycle life (¢ kWh^{-1} cyc^{-1}). The demonstration of long-life liquid metal batteries still remains; however, based upon similar three-liquid-layer industrial electrochemical systems, such as the Hoopes cell, one might expect continuous operational lifetimes in excess of 20 years to be possible.

It should be emphasized that grid storage is a multidimensional cost-based challenge. In fact, there is a spectrum of requirements that demand differing types of energy service, from high-power storage required by frequency response applications to bulk-energy storage that enables base-load renewable energy. We believe that liquid metal batteries are well positioned to simultaneously address multiple end-uses at a commercially competitive price. Specifically, liquid metal batteries currently produced at the laboratory-scale generally have cell electrode materials energy costs of $50−100 kWh^{-1} and power costs of $50−400 kW^{-1} when operated at current densities between 70 and 1100 mA cm^{-2}. Approximating for battery balance of system costs (typically on the order of four times the material costs), liquid metal batteries have the potential to outperform Pb-acid, Na−S, Ni−Cd, Li-ion, and various flow cell devices on both a cost per energy and cost per power basis, all before accounting for unknown economies of scale. This is only possible due to the unique design of the three-liquid-layer system, which enables rapid charge−discharge kinetics due to facile charge transfer, molten salt electrolyte enabled high rate capability, long-life imparted by robust liquid electrodes, and manufacturing scalability arising from the natural self-segregation of all-liquid components. All of these advantages are unique to the liquid metal battery and make it an attractive candidate for addressing a wide array of energy market opportunities.

When viewed holistically, the ability of energy storage to improve so many market segments lends credence to the belief that the greatest energy bottleneck of the modern day lies in the ability to store energy, not to generate it. Several authors have begun to highlight the inability of renewables to be considered as reliable base-load contributors, as well as the economic supply−demand vulnerabilities resulting from the saturation of renewables, without a suitable means of domestically providing base power during cloudy or windless periods.[188−190] Thus, grid-level energy storage opportunities like the liquid metal battery are truly a bridging technology between sustainable energy production and consumption.

The future of liquid metal batteries is particularly exciting, and the space for research is rich with opportunity. The combination of cost-driven development with a deep knowledge of the work that has proceeded is the formula to turn the concept of the liquid metal battery into a viable energy storage solution.

AUTHOR INFORMATION

Corresponding Author

*E-mail: dsadoway@mit.edu. Telephone: 617 253 3487. Fax: 617 253 5418.

Notes

The authors declare no competing financial interest.

Biographies

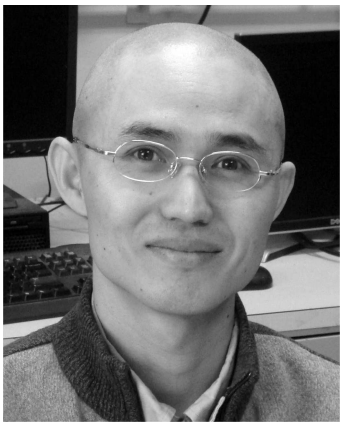

Dr. Hojong Kim is a research scientist at MIT, where he is leading efforts to develop electrode materials for use in liquid metal battery technology. His research interests include electrochemical energy conversion and storage, environment-friendly electrometallurgical processes, high-temperature corrosion, and materials for energy storage and conversion. Previously, he worked as a senior research scientist and project lead at Samsung Corning Precision Glass Co. Ltd to improve the process yield for thin film transistor liquid crystal display (TFT-LCD) glass manufacturing. Kim received his Ph.D. in the Uhlig Corrosion Laboratory at MIT under Professor Latanision

(2004) and B.S. in Materials Science and Engineering from Seoul National University in South Korea (2000).

Dr. Dane Boysen currently serves as a program director at the Advanced Research Projects Agency-Energy (ARPA-E). Prior to joining ARPA-E, Boysen led the development of the grid-scale energy storage liquid metal battery at MIT under Professor Donald Sadoway. In 2004, he cofounded Superprotonic Inc., a venture capital-backed start-up company dedicated to the commercialization of solid acid electrolyte-based fuel cells. This work has led to numerous patents and publications in eminent periodicals, such as *Science* (January 2004) and *Nature* (April 2001). His main focuses include electrochemical energy conversion and storage, natural gas conversion and storage technology, and materials for energy storage and conversion. Boysen received his M.S. (2001) and Ph.D. (2004) in Materials Science at the California Institute of Technology under Professor Sossina Haile.

Jocelyn Newhouse is a doctoral candidate in the Sadoway group where she studies the kinetic limitations of high temperature electrochemical alloying as it applies to the development of liquid metal batteries. Her research interests include large-scale energy storage, efficiency of the electricity grid, and integration of intermittent renewable energy sources. Prior to MIT, Jocelyn obtained a B.A. in Chemistry from Grinnell College, where she earned various awards and also studied Spanish and economics.

Brian Spatocco is currently a doctoral candidate in the Sadoway research group where he focuses on low-temperature, low-cost liquid metal battery solutions for grid-scaled storage. Prior to MIT, Spatocco obtained his B.S. in Materials Science and Engineering from Rutgers University and M.Phil. in Technology Enterprise from the University of Cambridge while on a Gates Cambridge Fellowship. His master's thesis studied the cost competitiveness and market compatibility of ionic liquid-based electrolytes for lithium ion batteries. Outside of energy research, Spatocco serves as a national and global student voice for graduate research support and was recently named a 2012 Kremlin Fellow for his targeted connection between the United States and Russia in the area of emerging energy market cooperation.

Dr. Brice Chung is currently the lead scientist on the liquid metal battery project for Total, a major partner of the research. Prior to beginning work on the liquid metal battery project in 2010, Chung earned his Ph.D. in theoretical physics from Université Paris Sud (2009) and a Masters in renewable energy from Mines Paris Tech (2010). After studying strongly correlated quantum states for his thesis work, Chung now focuses on innovation for clean energy, specifically in the field of materials and devices for energy conversion and storage. His current research efforts include the development of novel chemistries for liquid metal batteries and technology scale-up.

dx.doi.org/10.1021/cr300205k | *Chem. Rev.* 2013, 113, 2075−2099

Dr. Paul Burke currently leads the liquid metal battery energy storage project at MIT under Professor Donald Sadoway. Personal research efforts include cell scale-up and investigation of emerging chemistries. Before joining Group Sadoway at MIT, Burke focused on the development of magnesium powder metallurgy technology and continues to collaborate in the field. Other research interests include hydrometallurgical processing of electronic waste. Burke is a graduate of Dalhousie University in Halifax, NS, with a M.A.Sc. (2007) and Ph.D. (2011) under Professor Georges Kipouros.

Dr. David Bradwell currently serves as the CTO and senior vice president of commercialization for Ambri Inc., (formerly known as Liquid Metal Battery Corporation), a start-up company he cofounded to develop and commercialize liquid metal battery technology. Prior to joining Ambri, Bradwell was a Ph.D. student under Professor Sadoway in the Department of Materials Science and Engineering at MIT, where he launched the research on liquid metal batteries. After graduating, Bradwell worked as a postdoctoral research associate on the liquid metal battery project and ultimately took over as the project lead before transitioning to the company in late 2011. Bradwell won a TR35 award in 2010 for being one of the world's top 35 innovators under the age of 35.

Dr. Kai Jiang is currently a professor at Huazhong University of Science and Technology (HUST) in China. Prior to joining HUST, Jiang worked on the development of liquid metal batteries for grid-scale energy storage as a postdoctoral associate in the Department of Materials Science and Engineering at MIT. He also conducted research on organic photovoltaics as a visiting scholar at Auburn University between 2007 and 2009. Jiang received his B.S. (1999) in physical chemistry and Ph.D. (2006) in electrochemistry at Wuhan University, China. His current research interests focus on electrochemical energy storage and advanced materials for sustainable energy.

Dr. Alina A. Tomaszowska currently serves as a project manager at Procter & Gamble. She joined MIT as a postdoctoral research associate in 2010 under Professor Donald Sadoway, where her research focused on the development of electrolytes for grid-scale energy storage liquid metal battery. Prior to joining MIT, Tomaszowska completed her Ph.D. in Chemistry at the Queens University of Belfast under Professor Kenneth R. Seddon. Her studies focused on the synthesis, characterization and application of novel ionic liquids. Apart from her academic activities, Tomaszowska conducted technology due diligence and provided expertise in the synthesis and application of ionic liquids to industrial clients and investors. In 2006, Tomaszowska received her M.Eng. in Chemical Technology at The Silesian University of Technology, Poland.

Dr. Kangli Wang is currently working on the development of electrode materials for liquid metal batteries as a postdoctoral associate in Professor Donald Sadoway's group at MIT. From 2007 to 2010, she was a postdoctoral fellow in the group of Professor Jeffrey Fergus in Material Engineering at Auburn University. She received her B.S. in chemistry from Hubei University, China, in 2001 and her Ph.D. in electrochemistry from Wuhan University, China, in 2006. Her research interests include electrochemical energy storage, electrocatalysis, and electrochemical sensors.

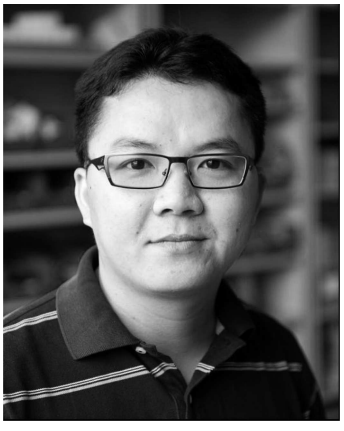

Dr. Weifeng Wei is currently a professor of Materials Engineering in the State Key Laboratory for Powder Metallurgy at the Central South University (China). After receiving his Ph.D. in Materials Engineering from the University of Alberta (2009), Wei joined the Sadoway Group as a postdoctoral research associate. His research concerns materials development in the fields of energy conversion and storage, including materials and device development for electrochemical energy storage devices, such as electrochemical supercapacitors and Li-ion rechargeable batteries, and electrochemical recycling of spent materials in molten salt electrolytes. He has published more than 30 refereed journal papers and presented at many conferences.

Luis Ortiz, Sc.D., is cofounder of Liquid Metal Battery Corporation (LMBC). Prior to founding LMBC, Luis served as research director for the Sadoway research group from 2008 to 2011. An accomplished technologist, Luis has 6 years of industrial experience in the battery industry serving as both an independent consultant and program manager for technology transfer while with Valence Technology. Prior to entering the energy sector, Luis was a Six Sigma Black Belt in Honeywell's Electronic Materials Division. Luis received an S.B. and Sc.D. from MIT's Department of Materials Science and Engineering.

Salvador Barriga is currently a doctoral candidate in the department of Materials Science and Engineering at MIT working under Donald Sadoway. His research focuses on electrochemical measurement of diffusivity in liquid alloys and development of multiphysics computational models for liquid metal battery systems. Barriga previously researched chemical adsorption of molybdenum selenide nanowires, SQUID-detected magnetic resonance imaging, microfabrication of bolomoters, and characterization of single photon detectors called avalanche photodiodes. He also holds numerous leadership awards, including the John Wulff Award for Excellence in Teaching from his department. Barriga received his B.A. (2006) in physics at the University of California, Berkeley, and his A.S. (2004) in physical science at Modesto Junior College.

dx.doi.org/10.1021/cr300205k | *Chem. Rev.* 2013, 113, 2075−2099

Dr. Sophie Poizeau is currently a postdoctoral associate in Materials Science and Engineering at MIT, working under the mentorship of Prof. Sadoway. Her research focuses on the thermodynamic properties of liquid alloys, involving both experimental work and thermodynamic modeling, for the development of liquid metal batteries. She conducted her doctoral studies at MIT in the Sadoway group and holds an engineering degree (M. Eng. equivalent) from the École Centrale Paris in France, from which she graduated in 2008.

Dr. Donald Sadoway is the John F. Elliott Professor of Materials Chemistry in the Department of Materials Science and Engineering at MIT. The author of over 140 scientific papers and holder of 18 U.S. patents, his research into the electrochemistry of molten salts has resulted in the invention of a rechargeable battery for grid-level storage applications and the development of environmentally sound electrochemical technology for the extraction, refining, and recycling of metals. Sadoway obtained the B.A.Sc. in Engineering Science, the M.A.Sc. in Chemical Metallurgy, and the Ph.D. in Chemical Metallurgy, all from the University of Toronto. From 1995 to 2005, he held a MacVicar Faculty Fellowship, MIT's highest award for excellence in undergraduate education. In 2001, he was elected Member of the Norwegian Academy of Technological Sciences. In 2012, he was named by Time magazine as one of the "100 Most Influential People in the World".

ACKNOWLEDGMENTS

The authors thank Professor Elton J. Cairns for sharing his valuable insight, experience, and knowledge with the MIT research team. The financial support of the US Department of Energy, Advanced Research Projects Agency-Energy (Award No. DE-AR0000047) and TOTAL, S.A., is gratefully acknowledged.

GLOSSARY

Symbols

η_{carnot}	Carnot cycle efficiency
η_{ct}	charge transfer losses
η_{ohm}	ohmic losses
η_{mt}	mass transport losses
ρ_i	density of component i
ρ_m	liquid density at melting temperature
σ	electrical conductivity
σ_i	volatility of the metal price
a_i	activity of species i
C_E^{est}	estimated cost of energy
C_E^{real}	realized cost of energy
C_P^{real}	realized cost of power
E_{cell}	operating cell voltage
$\hat{E}_{cell}$	average cell discharge voltage
$E_{cell,eq}$	equilibrium cell potential
$\hat{E}_{cell,eq}$	average equilibrium cell voltage
E_c	full-charge cell voltage
E_d	full-discharge cell voltage
E_{th}	thermoneutral potential
F	Faraday constant
$\Delta_r G^\circ$	standard change in Gibbs free energy of reaction
$\Delta\bar{G}_{cell}$	partial molar Gibbs free energy of the cell
$\bar{G}_i$	partial molar Gibbs free energy of species i
$\Delta_r H^\circ$	standard change in enthalpy of reaction
$\Delta\bar{H}_{cell}$	partial molar enthalpy of the cell
I	current
j	area specific current density
K_{eq}	equilibrium constant
m	number of months
n_i	moles of species i
$\dot{n}_A$	molar oxidation/reduction rate of reactant A
$\hat{P}_{i,j}$	average price of month j for electrode material i
$\hat{P}_i$	average monthly bulk metal market price
Q_d	measured cell discharge capacity
$\dot{Q}_{gen}$	total rate of heat generation
$\dot{Q}_{irr}$	rate of irreversible heat generation
$\dot{Q}_{loss}$	rate of heat loss
$\dot{Q}_{rev}$	rate of reversible entropic heat absorbed or generated
R	gas constant
$\Delta\bar{S}_{cell}$	partial molar entropy of the cell
T	temperature
T_b	boiling temperature
T_m	melting temperature
$T_{liquidus}$	liquidus temperature
x_i	mole fraction of species i
w_i	mass fraction of component i
z	number of electrons in an electrochemical reaction or charge number of an ion

Acronyms

SHE	standard hydrogen electrode
CAES	compressed air energy storage
GM	General Motors Corporation
ANL	Argonne National Laboratory
AI	Atomics International
MIT	Massachusetts Institute of Technology
ZEBRA	Zeolite Battery Research Africa

REFERENCES

(1) Chalamala, B. R. *Proc. IEEE* **2007**, *95*, 2106.

(2) Bard, A. J.; Parsons, R.; Jordan, J. *Standard Potentials in Aqueous Solution*; Marcel Dekker: New York, 1985.
(3) Stender, W. W.; Zivotinsky, P. B.; Stroganoff, M. M. *Trans. Electrochem. Soc.* **1934**, *65*, 189.
(4) Bard, A. J.; Faulkner, L. R. *Electrochemical Methods: Fundamentals and Applications*; John Wiley: New York, 2001.
(5) Christensen, J.; Newman, J. *J. Solid State Electrochem.* **2006**, *10*, 293.
(6) Deshpande, R. D.; Li, J. C.; Cheng, Y. T.; Verbrugge, M. W. *J. Electrochem. Soc.* **2011**, *158*, A845.
(7) Eyer, J.; Corey, G. Energy Storage for the Electricity Grid: Benefits and Market Potential Assessment Guide - A Study for the DOE Energy Storage Systems Program, SAND2010-0815; Sandia National Laboratories: Livermore, CA, 2010.
(8) Rastler, D. Electricity Energy Storage Technology Options: A White Paper Primer on Applications, Costs, and Benefits, report number 1020676; Electric Power Research Institute: Palo Alto, 2010.
(9) Schoenung, S. Energy Storage Systems Cost Update: A Study for the DOE Energy Storage Systems Program, SAND2011-2730; Sandia National Laboratories: Livermore, CA, 2011.
(10) Electricity Storage Association. http://www.electricitystorage.org/ (accessed Dec. 2011).
(11) Yang, Z. G.; Zhang, J. L.; Kintner-Meyer, M. C. W.; Lu, X. C.; Choi, D. W.; Lemmon, J. P.; Liu, J. *Chem. Rev.* **2011**, *111*, 3577.
(12) Hoopes, W. Electrolytically-refined Aluminum and Articles Made Therefrom. U.S. Patent 1,534,315, 1925.
(13) Kondo, M.; Maeda, H.; Mizuguchi, M. *JOM* **1990**, *42*, 36.
(14) Sanders, R. E. *Kirk-Othmer Encyclopedia of Chemical Technology*; John Wiley & Sons, Inc.: New York, 2000; Vol. *2*.
(15) Van, T. D.; Segers, L.; Winand, R. *J. Electrochem. Soc.* **1994**, *141*, 927.
(16) Kondo, M.; Imamaki, T. The Production Method and the Properties of High Purity Aluminum Refined by Three Layer Electrolytic Refining Process, Presented at the Light metal symposium (Keikinzoku Gakkai Symposium), Japan, 1998.
(17) Yeager, E. Fuel Cells: Basic Considerations, in Power Sources Division, *Proceedings of 12th Annual Battery Research and Development*; Army Signal Research & Development Laboratory: Fort Monmouth, NJ, 21−22 MAY, 1958; p 2.
(18) *Regenerative EMF Cells*; Crouthamel, C. E., Recht, H. L., Eds.; Advances in Chemistry, Vol. *64*; American Chemical Society: Washington, DC, 1967.
(19) Agruss, B. Regenerative Battery. U.S. Patent 3,245,836, 1966.
(20) Weaver, R. D.; Smith, S. W.; Willmann, N. L. *J. Electrochem. Soc.* **1962**, *109*, 653.
(21) Agruss, B. *J. Electrochem. Soc.* **1963**, *110*, 1097.
(22) Agruss, B.; Karas, H, R. In *Regenerative EMF Cells*; Crouthamel, C. E., Recht, H. L., Eds.; Advances in Chemistry, Vol. *64*; American Chemical Society: Washington, DC, 1967; pp 62−81.
(23) Agruss, B.; Karas, H. R. First Quarterly Technical Progress Report on Design and Develpment of a Liquid Metal Cell, 274197; General Motors Corporation: Indianapolis, Inidana, 1962.
(24) Groce, I. J.; Oldenkamp, R. D. In *Regenerative EMF Cells*; Crouthamel, C. E., Recht, H. L., Eds.; Advances in Chemistry, Vol. *64*; American Chemical Society: Washington, DC, 1967; pp 43−52.
(25) Heredy, L. A.; Iverson, M. L.; Ulrich, G. D.; Recht, H. L. In *Regenerative EMF Cells*; Crouthamel, C. E., Recht, H. L., Eds.; Advances in Chemistry, Vol. *64*; American Chemical Society: Washington, DC, 1967; pp 30−42.
(26) Oldenkamp, R. D.; Recht, H. L. In *Regenerative EMF Cells*; Crouthamel, C. E., Recht, H. L., Eds.; Advances in Chemistry, Vol. *64*; American Chemical Society: Washington, DC, 1967; pp 53−61.
(27) Fischer, A. K. In *Regenerative EMF Cells*; Crouthamel, C. E., Recht, H. L., Eds.; Advances in Chemistry, Vol. *64*; American Chemical Society: Washington, DC, 1967; pp 121−135.
(28) Foster, M. S. In *Regenerative EMF Cells*; Crouthamel, C. E., Recht, H. L., Eds.; Advances in Chemistry, Vol. *64*; American Chemical Society: Washington, DC, 1967; pp 136−148.
(29) Hesson, J. C.; Shimotake, H. In *Regenerative EMF Cells*; American Chemical Society, 1967; Vol. *64*, pp 82−104.
(30) Johnson, C. E.; Heinrich, R. R. In *Regenerative EMF Cells*; Crouthamel, C. E., Recht, H. L., Eds.; Advances in Chemistry, Vol. *64*; American Chemical Society: Washington, DC, 1967; pp 105−120.
(31) Lawroski, S.; Vogel, R.; Levenson, M.; Munnecke, V. Chemical Engineering Division Summary Report, ANL-6543; Argonne National Laboratory: Chicago, 1962.
(32) Lawroski, S.; Vogel, R.; Levenson, M.; Munnecke, V. Chemical Engineering Division Summary Report, ANL-6687; Argonne National Laboratory: Chicago, 1963.
(33) Lawroski, S.; Vogel, R.; Levenson, M.; Munnecke, V. Chemical Engineering Division Semiannual Report, ANL-6800; Argonne National Laboratory: Chicago, 1963.
(34) Lawroski, S.; Vogel, R.; Levenson, M.; Masten, F. Chemical Engineering Division Semiannual Report, ANL-6925; Argonne National Laboratory: Chicago, 1964.
(35) Vogel, R.; Levenson, M.; Masten, F. Chemical Engineering Division Semiannual Report, ANL-7055, Argonne National Laboratory: Chicago, 19641965.
(36) Vogel, R.; Levenson, M.; Schraidt, J.; Royal, J. Chemical Engineering Division Semiannual Report; ANL-7125; Argonne National Laboratory: Chicago, 1966.
(37) Cairns, E. J.; Crouthamel, C. E.; Fischer, A. K.; Foster, M. S.; Hesson, J. C. Galvanic cells with fused salts, ANL-7316; Argonne National Laboratory: Chicago, 1967.
(38) Vogel, R.; Levenson, M.; Proud, E.; Royal, J. Chemical Engineering Division Semiannual Report, ANL-7325; Argonne National Laboratory: Chicago, 1967.
(39) Vogel, R. C.; Levenson, M.; Schraidt, J. H.; Royal, J. *Chemical Engineering Division Semiannual Report*; ANL-7125; Argonne National Laboratory: Chicago, 1966.
(40) Shimotake, H.; Cairns, E. J. Bimetallic Galvanic Cells with Fused Salt Electrolyte. *Intersociety Energy Conversion Engineering Conference Proceedings*; American Society of Mechanical Engineers: New York, 1967.
(41) Shimotak., H; Cairns, E. J. *IEEE Trans. Electron Devices* **1968**, *ED15*, 803.
(42) Cairns, E. J.; Shimotake, H. *Science* **1969**, *164*, 1347.
(43) Cairns, E. J.; Kyle, M. L.; Maroni, V. A.; Shimotake, H.; Steunenberg, R. K.; Tevebaugh, A. D. Development of High Energy Batteries for Electric Vehicles, ANL-7756; Argonne National Laboratory: Chicago, 1970.
(44) Cairns, E. J.; Gay, E. C.; Kolba, V. M.; Kyle, M. L.; Tevebaugh, A. D.; Trevorrow, L. E. Lithium Selenium Secondary Cells for Components in Electric Vehiculary Propulsion Generating Systems, ANL-7745; Argonne National Laboratory: Chicago, 1970.
(45) Cairns, E. J.; Cafasso, F. A.; Cunningham, P. T.; Eberhart, J. G.; Feder, H. M.; Maroni, V. A.; Schnyders, H. C.; Veleckis, E.; Tevebaugh, A. D.; Vogel, R. C. Physical Chemistry of Liquid Metals and Molten Salts-Semiannual Report, ANL-7823; Argonne National Laboratory: Chicago, 1971.
(46) Cairns, E. J.; Steunenberg, R. K.; Ackerman, J. P.; Feay, B. A.; Gruen, D. M.; Kyle, M. L.; Latimer, T. W.; Mundy, J. N.; Rubischko, R.; Shimotake, H.; Walker, D. E.; Zielen, A. J.; Tevebaugh, A. D. Development of High Energy Batteries for Electric Vehicles, ANL-7888; Argonne National Laboratory: Chicago, 1971.
(47) Cunningham, P. T.; Johnson, S. A.; Cairns, E. J. *J. Electrochem. Soc.* **1971**, *118*, 1941.
(48) Cairns, E. J.; Gay, E. C.; Steunenberg, R. K.; Shimotake, H.; Selman, J. R.; Wilson, T. L.; Webster, D. S. Development of High Specific Energy Batteries for Electric Vehicles, ANL-7953; Argonne National Laboratory: Chicago, 1972.
(49) Gay, E. C.; Arntzen, J. D.; Cairns, E. J.; Kincinas, J. E.; Riha, J. G.; Trevorrow, L. E.; Walsh, W. J.; Webster, D. S. Lithium Chalcogen Secondary Cells for Components in Electric Vehicular Propulsion Generating Systems, ANL-7863; Argonne National Laboratory: Chicago, 1972.

(50) Cunningham, P. T.; Cairns, E. J.; Johnson, S. A. *J. Electrochem. Soc.* **1972**, *119*, 1448.
(51) Kyle, M. L.; Webster, D. S.; Cairns, E. J. Lithium Sulfur Batteries for Off-peak Energy Storage and Peak Power Generation Systems, ANL-7958; Argonne National Laboratory: Chicago, 1973.
(52) Cairns, E. J.; Nelson, P. A.; Gay, E. C.; Steunenberg, R. K.; Walsh, W. J.; Battles, J. E.; Shimotake, H.; Ackerman, J. P.; Kyle, M. L.; Webster, D. S. Development of High Specific Energy Batteries for Electric Vehicles, ANL-7998; Argonne National Laboratory: Chicago, 1973.
(53) Walsh, W. J.; Gay, E. C.; Arntzen, J. D.; Kincinas, J. E.; Cairns, E. J.; Webster, D. S. Lithium Chalcogen Secondary Cells for Components in Electric Vehicular Propulsion Generation Systems, ANL-7999; Argonne National Laboratory: Chicago, 1973.
(54) Cunningham, P. T.; Cairns, E. J.; Hathaway, E. J.; Johnson, S. A.; Maroni, V. A. *J. Electrochem. Soc.* **1973**, *120*, 591.
(55) Cunningham, P. T.; Johnson, S. A.; Cairns, E. J. *J. Electrochem. Soc.* **1973**, *120*, 328.
(56) Cairns, E. J.; Kucera, G. H.; Cunningh., Pt *J. Electrochem. Soc.* **1973**, *120*, 595.
(57) Nelson, P. A.; Barney, D. L.; Steunenberg, R. K.; Chilenskas, A. A.; Gay, E. C.; Battles, J. E.; Hornstra, F.; Miller, W. E.; Roche, M. F.; Shimotake, H.; Hudson, R.; Rubischko, R. J.; Sudar, S. High-Performance Batteries for Electric-Vehicle Propulsion and Stationary Energy Storage, ANL-78-94; Argonne National Laboratory: Chicago, 1978.
(58) Nelson, P. A.; Barney, D. L.; Steunenberg, R. K.; Chilenskas, A. A.; Gay, E. C.; Battles, J. E.; Hornstra, F.; Miller, W. E.; Vissers, D. R.; Roche, M. F.; Shimotake, H.; Hudson, R.; Rubischko, R. J.; Sudar, S. High-Performance Batteries for Electric-Vehicle Propulsion and Stationary Energy Storage, ANL-79-39; Argonne National Laboratory: Chicago, 1979.
(59) Barney, D. L.; Roche, M. F.; Preto, S. K.; Ross, L. E.; Otto, N. C.; Martino, F. J. Calcium/Metal Sulfide Battery Development Program, ANL-81-14; Argonne National Laboratory: Chicago, 1981.
(60) Sudworth, J. L. *Philos. Trans. R. Soc. London, Ser. A* **1996**, *354*, 1595.
(61) Kummer, J. T.; Weber, N. *Proc. SAE Congr.* **1967**, 670179.
(62) Kummer, J. T.; Weber, N. Battery Having a Molten Alkali Metal Anode and a Molten Sulfur Cathode. U.S. Patent 3,413,150, 1968.
(63) Sudworth, J. L.; Tilley, A. R. *The Sodium Sulfur Battery*; Chapman & Hall: London, New York, 1985.
(64) Sudworth, J. L.; Barrow, P.; Dong, W.; Dunn, B.; Farrington, G. C.; Thomas, J. O. *MRS Bull.* **2000**, *25*, 22.
(65) Kyle, M. L.; Webster, D. S.; Cairns, E. J. *J. Electrochem. Soc.* **1972**, *119*, C214.
(66) Cairns, E. J., Lawrence Berkeley National Laboratory, Berkeley, CA, Personal communication, 2011.
(67) Armbruster, M. H.; Crenshaw, J. L. *J. Am. Chem. Soc.* **1934**, *56*, 2525.
(68) Lantratov, M. F.; Alabyshev, A. F. *Zh. Fiz. Khim.* **1959**, *33*, 2429.
(69) Lantratov, M. F.; Tsarenko, E. V. *Zh. Fiz. Khim.* **1959**, *33*, 1792.
(70) Lantratov, M. F. *Zh. Fiz. Khim.* **1960**, *34*, 782.
(71) Terpilow, J.; Barycka, I. *Bull. Acad. Pol. Sci., Ser. Sci. Chim.* **1961**, *9*, 175.
(72) Terpilowski, J.; Slaby, H. *Bull. Acad. Pol. Sci., Ser. Sci. Chim.* **1963**, *11*, 317.
(73) Slaby, H.; Terpilow., J *Bull. Acad. Pol. Sci., Ser. Sci. Chim.* **1964**, *12*, 581.
(74) Chiotti, P.; Stevens, E. R. *Trans. Metall. Soc. AIME* **1965**, *233*, 198.
(75) Iverson, M. L.; Recht, H. L. *J. Chem. Eng. Data* **1967**, *12*, 262.
(76) Chiotti, P.; Hecht, R. J. *Trans. Metall. Soc. AIME* **1967**, *239*, 536.
(77) Belton, G. R.; Rao, Y. K. *Trans. Metall. Soc. AIME* **1969**, *245*, 2189.
(78) Yuan, D.; Kroger, F. A. *J. Phys. Chem.* **1969**, *73*, 2390.
(79) Nebell, H. *Rev. Roum. Chim.* **1970**, *15*, 59.
(80) Morachevskii, A. G.; Bykova, M. A.; Rozova, T. T. *Zh. Prikl. Khim.* **1970**, *43*, 1611.
(81) Lantratov, M. F.; Mikhailova, A. G. *Zh. Prikl. Khim.* **1971**, *44*, 1778.
(82) Hsueh, L.; Bennion, D. N. *J. Electrochem. Soc.* **1971**, *118*, 1128.
(83) Pogodaev, A. M.; Lukashenko, E. E. *Russ. J. Phys. Chem.* **1972**, *46*, 197.
(84) Bykova, M. A.; Morachev, A. G. *Zh. Prikl. Khim.* **1973**, *46*, 312.
(85) Egan, J. J. *J. Nucl. Mater.* **1974**, *51*, 30.
(86) Fray, D. J.; Savory, B. *J. Chem. Thermodyn.* **1975**, *7*, 485.
(87) Delcet, J.; Egan, J. J. *Metall. Trans. B* **1978**, *9*, 728.
(88) Delcet, J.; Egan, J. J. *J. Less-Common Met.* **1978**, *59*, 229.
(89) Delcet, J.; Heus, R. J.; Egan, J. J. *J. Electrochem. Soc.* **1978**, *125*, 755.
(90) Rivier, M.; Pelton, A. D. *J. Electrochem. Soc.* **1978**, *125*, 1377.
(91) Weppner, W.; Huggins, R. A. *J. Electrochem. Soc.* **1978**, *125*, 7.
(92) Wen, C. J.; Boukamp, B. A.; Huggins, R. A.; Weppner, W. *J. Electrochem. Soc.* **1979**, *126*, 2258.
(93) Tamaki, S.; Cusack, N. E. *J. Phys. F: Met. Phys.* **1979**, *9*, 403.
(94) Predel, B.; Hulse, K. *J. Less-Common Met.* **1979**, *63*, 159.
(95) Delcet, J.; Delgado-Brune, A.; Egan, J. J. Coulometric Titrations Using CaF2 and BaF2 Solid Electrolytes to Study Alloy Phases, *Proceedings of the Symposium on Calculation of Phase Diagrams and Thermochemistry of Alloy Phases, Milwaukee, WI*; Metallurgical Society of AIME: Englewood, CO, 1979; p 275.
(96) Delcet, J.; Brune, A.; Egan, J. J. *J. Met.* **1979**, *31*, F37.
(97) Wen, C. J.; Huggins, R. A. *Mater. Res. Bull.* **1980**, *15*, 1225.
(98) Gray, P.; Cusack, N. E.; Tamaki, S.; Tsuchiya, Y. *Phys. Chem. Liq.* **1980**, *9*, 307.
(99) Wen, C. J.; Huggins, R. A. *J. Solid State Chem.* **1980**, *35*, 376.
(100) Wen, C. J.; Huggins, R. A. *J. Electrochem. Soc.* **1981**, *128*, 1181.
(101) Wen, C. J.; Huggins, R. A. *J. Electrochem. Soc.* **1981**, *128*, 1636.
(102) Wen, C. J.; Huggins, R. A. *J. Solid State Chem.* **1981**, *37*, 271.
(103) Ishiguro, T.; Takeda, S.; Tamaki, S. *J. Phys. F: Met. Phys.* **1982**, *12*, 845.
(104) Notin, M.; Djamshidi, B.; Gachon, J. C.; Hertz, J. *Thermochim. Acta* **1982**, *57*, 57.
(105) Notin, M.; Gachon, J. C.; Hertz, J. *J. Less-Common Met.* **1982**, *85*, 205.
(106) Notin, M.; Gachon, J. C.; Hertz, J. *J. Chem. Thermodyn.* **1982**, *14*, 425.
(107) Notin, M.; Hertz, J. *CALPHAD: Comput. Coupling Phase Diagrams Thermochem.* **1982**, *6*, 49.
(108) Rais, A.; Cusack, N. E.; Neale, F. E. *J. Phys. F: Met. Phys.* **1982**, *12*, 1091.
(109) Tamaki, S.; Ishiguro, T.; Takeda, S. *J. Phys. F: Met. Phys.* **1982**, *12*, 1613.
(110) Morachesvkii, A. G.; Maiorova, E. A.; Romanchenko, N. M.; Kozlova, M. V. *Russ. J. Appl. Chem.* **1982**, *55*, 481.
(111) Matsunaga, S.; Ishiguro, T.; Tamaki, S. *J. Phys. F: Met. Phys.* **1983**, *13*, 587.
(112) Eckert, C. A.; Irwin, R. B.; Smith, J. S. *Metall. Trans. B* **1983**, *14*, 451.
(113) Iwase, M.; Sugino, S.; Ichise, E. *High Temp. Mater. Processes (London)* **1984**, *6*, 143.
(114) Iwase, M.; Sugino, S.; Ichise, E.; Waseda, Y. *J. Chem. Thermodyn.* **1985**, *17*, 601.
(115) Egan, J. J.; Freyland, W. *Ber. Bunsen-Ges.* **1985**, *89*, 381.
(116) Egan, J. J. *High Temp. Sci.* **1985**, *19*, 111.
(117) Saboungi, M. L.; Leonard, S. R.; Ellefson, J. *J. Chem. Phys.* **1986**, *85*, 6072.
(118) Petric, A.; Pelton, A. D.; Saboungi, M. L. *J. Electrochem. Soc.* **1988**, *135*, 2754.
(119) Petric, A.; Pelton, A. D.; Saboungi, M. L. *J. Chem. Phys.* **1988**, *89*, 5070.
(120) Petric, A.; Pelton, A. D.; Saboungi, M. L. *J. Phys. F: Met. Phys.* **1988**, *18*, 1473.
(121) Saboungi, M. L.; Ellefson, J.; Johnson, G. K. *J. Chem. Phys.* **1988**, *88*, 5812.
(122) Srikanth, S.; Jacob, K. T. *Metall. Trans. B* **1991**, *22*, 607.

(123) Takenaka, T.; Petric, A.; Saboungi, M. L. *J. Phys.: Condens. Matter* **1991**, *3*, 1603.
(124) Srikanth, S.; Jacob, K. T. *Z. Metallkd.* **1991**, *82*, 675.
(125) Gasior, W.; Moser, Z. *J. Chim. Phys. Phys.-Chim. Biol.* **1993**, *90*, 387.
(126) Morachevskii, A. C.; Bochagina, E. V. *Russ. J. Appl. Chem.* **2000**, *73*, 952.
(127) Morachevskii, A. G. *Russ. J. Appl. Chem.* **2000**, *73*, 2017.
(128) Morachevskii, A. G.; Bochagina, E. B.; Bykova, M. A. *Russ. J. Appl. Chem.* **2000**, *73*, 1699.
(129) Morachevskii, A. G.; Bochagina, E. V. *Russ. J. Appl. Chem.* **2000**, *73*, 1875.
(130) Morachevskii, A. G.; Bochagina, E. V. *Russ. J. Appl. Chem.* **2000**, *73*, 1146.
(131) Morachevskii, A. G.; Bochagina, E. V. *Russ. J. Appl. Chem.* **2000**, *73*, 760.
(132) Morachevskii, A. G.; Vaisgant, Z. I.; Bochagina, E. V. *Russ. J. Appl. Chem.* **2000**, *73*, 391.
(133) Morachevskii, A. G. *Russ. J. Appl. Chem.* **2001**, *74*, 1994.
(134) Morachevskii, A. G. *Russ. J. Appl. Chem.* **2001**, *74*, 564.
(135) Morachevskii, A. G. *Russ. J. Appl. Chem.* **2001**, *74*, 569.
(136) Morachevskii, A. G.; Bykova, M. A. *Russ. J. Appl. Chem.* **2001**, *74*, 1793.
(137) Gasior, W.; Moser, Z. *J. Nucl. Mater.* **2001**, *294*, 77.
(138) Morachevskii, A. G. *Russ. J. Appl. Chem.* **2002**, *75*, 367.
(139) Morachevskii, A. G.; Bochagina, E. V. *Russ. J. Appl. Chem.* **2002**, *75*, 362.
(140) Huggins, R. A. *Energy Storage*; Springer: New York, London, 2010.
(141) Kim, H.; Boysen, D. A.; Bradwell, D. J.; Chung, B.; Jiang, K.; Tomaszowska, A. A.; Wang, K.; Wei, W.; Sadoway, D. R. *Electrochim. Acta* **2012**, *60*, 154.
(142) MetalPrices Online Database. http://www.metalprices.com (accessed Dec. 2011).
(143) *CRC Handbook of Chemistry and Physics*; CRC Press: Cleveland, OH, 1977.
(144) Massalski, T. B. *Binary Alloy Phase Diagrams*; ASM International: Materials Park, OH, 1990.
(145) Sitte, W.; Weppner, W. *Appl. Phys. A: Solids Surf.* **1985**, *38*, 31.
(146) Sitte, W.; Weppner, W. *Z. Naturforsch., A: Phys. Sci.* **1987**, *42*, 1.
(147) Bronstein, H. R.; Bredig, M. A. *J. Am. Chem. Soc.* **1958**, *80*, 2077.
(148) Ukshe, E. A.; Bukun, N. G. *Russ. Chem. Rev.* **1961**, *30*, 90.
(149) Bredig, M. A. Mixtures of Metals with Molten Salts, ORNL-3391; Oak Ridge National Laboratory: Oak Ridge, TN, 1963.
(150) Haarberg, G. M.; Thonstad, J. *J. Appl. Electrochem.* **1989**, *19*, 789.
(151) Haarberg, G. M.; Osen, K. S.; Heus, R. J.; Egan, J. J. *J. Electrochem. Soc.* **1990**, *137*, 2777.
(152) Bredig, M. A.; Bronstein, H. R.; Smith, W. T. *J. Am. Chem. Soc.* **1955**, *77*, 1454.
(153) Bredig, M. A.; Johnson, J. W.; Smith, W. T. *J. Am. Chem. Soc.* **1955**, *77*, 307.
(154) Johnson, J. W.; Bredig, M. A. *J. Phys. Chem.* **1958**, *62*, 604.
(155) Bredig, M. A.; Bronstein, H. R. *J. Phys. Chem.* **1960**, *64*, 64.
(156) Bredig, M. A.; Johnson, J. W. *J. Phys. Chem.* **1960**, *64*, 1899.
(157) Dworkin, A. S.; Bredig, M. A.; Bronstein, H. R. *Discuss. Faraday Soc.* **1961**, 188.
(158) Dworkin, A. S.; Bredig, M. A.; Bronstein, H. R. *J. Phys. Chem.* **1962**, *66*, 572.
(159) Lichter, B. D.; Bredig, M. A. *J. Electrochem. Soc.* **1965**, *112*, 506.
(160) Dworkin, A. S.; Bronstei, H. R.; Bredig, M. A. *J. Phys. Chem.* **1968**, *72*, 1892.
(161) Sharma, R. A. *J. Phys. Chem.* **1970**, *74*, 3896.
(162) Seefurth, R. N.; Sharma, R. A. *J. Electrochem. Soc.* **1975**, *122*, 1049.
(163) Delimarskii, I. K.; Markov, B. F. *Electrochemistry of Fused Salts*; Translated from the Russian by Adam Peiperl. Translation edited by Reuben E. Wood; Sigma Press: Washington DC, 1961.
(164) Vanartsdalen, E. R.; Yaffe, I. S. *J. Phys. Chem.* **1955**, *59*, 118.
(165) Johnson, C. E.; Hathaway, E. J. *J. Electrochem. Soc.* **1971**, *118*, 631.
(166) Janz, G. J.; Tomkins, R. P. T.; Allen, C. B. *J. Phys. Chem. Ref. Data* **1979**, *8*, 125.
(167) Bader, M.; Busse, C. A. *J. Nucl. Mater.* **1977**, *67*, 295.
(168) Bradwell, D. J.; Kim, H.; Sirk, A. H. C.; Sadoway, D. R. *J. Am. Chem. Soc.* **2012**, *134*, 1895.
(169) Linden, D.; Reddy, T. B. *Handbook of Batteries*; McGraw-Hill: New York, 2002.
(170) Guidotti, R. A.; Masset, P. *J. Power Sources* **2006**, *161*, 1443.
(171) Guidotti, R. A.; Masset, P. J. *J. Power Sources* **2008**, *183*, 388.
(172) DiStefano, J. R.; Hoffman, E. E. Corrosion Mechanisms in Refractory Metal-Alkali Metal Systems, ORNL-3424; Oak Ridge National Laboratory, 1963.
(173) *Liquid Metals Handbook*; US Government Printing Office: Washington DC, 1955.
(174) Manly, W. D. Fundamentals of Liquid Metal Corrosion, ORNL-2055; Oak Ridge National Laboratory, 1956.
(175) Vrana, L. M. *Kirk-Othmer Encyclopedia of Chemical Technology*; John Wiley & Sons, Inc.: New York, 2000.
(176) Janz, G. J.; Tomkins, R. P. T. *Corrosion* **1979**, *35*, 485.
(177) Shimotake, H.; Hesson, J. C. In *Regenerative EMF Cells*; Crouthamel, C. E., Recht, H. L., Eds.; Advances in Chemistry, Vol. *64*; American Chemical Society: Washington, DC, 1967; pp 149−185.
(178) Hesson, J. C. Seal. U.S. Patent 3,419,432, 1968.
(179) Oshima, T.; Kajita, M.; Okuno, A. *Int. J. Appl. Ceram. Technol.* **2004**, *1*, 269.
(180) Sudworth, J. L. *J. Power Sources* **2001**, *100*, 149.
(181) Bito, A. Overview of the Sodium-Sulfur Battery for the IEEE Stationary Battery Committee, Power Engineering Society General Meeting, 12−16 June, 2005; p 1232.
(182) Baker, D. J.; Budgen, W. G.; Smith, P. R. Joining of Ceramic Components to Metal Components. U.S. Patent 5,009,357, 1991.
(183) Kaun, T. D.; Hash, M. C.; Simon, D. R. Sulfide Ceramics in Molten Salt Electrolyte Batteries, ANL-84744; Argonne National Laboratory: Chicago, 1995.
(184) Kaun, T. D.; Nelson, P. A.; Redey, L.; Vissers, D. R.; Henriksen, G. L. *Electrochim. Acta* **1993**, *38*, 1269.
(185) Henriksen, G. L.; Vissers, D. R. *J. Power Sources* **1994**, *51*, 115.
(186) Jansen, A.; Henriksen, G. L.; Nelson, P. A., Argonne National Laboratory, Lemont, IL, Private communication, 2011.
(187) Okuyama, R.; Nomura, E. *J. Power Sources* **1999**, *77*, 164.
(188) Rosenbloom, E. A Problem With Wind Power; http://www.aweo.org/problemwithwind.html, 2006.
(189) DeMeo, E. A.; Jordan, G. A.; Kalich, C.; King, J.; Milligan, M. R.; Murley, C.; Oakleaf, B.; Schuerger, M. J. *IEEE Power Energy Mag.* **2007**, *5*, 59.
(190) Denholm, P.; Ela, E.; Kirby, B.; Milligan, M. The Role of Energy Storage with Renewable Electricity Generation, NREL/TP-6A2-47187; National Renewable Energy Laboratory: Golden, CO, 2010.